

ORIGINAL PAPER

Open Access



The Erdmannshöhle near Hasel, SW Germany: karst environment and cave evolution

Arnfried Becker^{1*}, Karsten Piepjohn² and Andrea Schröder-Ritzrau³

Abstract

The Erdmannshöhle is located at the NE margin of the Dinkelberg plateau in SW Germany. With a length of 2315 m, it is the longest cave in the deep open karst area near the village of Hasel. Three main cave levels developed in moderately SW-dipping, thinly bedded and fractured limestones of the Upper Muschelkalk (Triassic). The youngest cave level containing the cave stream is still active. Eighteen samples for U/Th dating were taken from the oldest and the intermediate cave levels. At the oldest cave level, the ages range from 162 to 110 ka, indicating speleothem growth starting in the middle Beringen Glaciation and terminating at the end of the Eem Interglacial. At the intermediate cave level, the ages range from 100 to 12 ka, i.e. early Birrfeld Glaciation to Younger Dryas Stadial. The age dating shows that speleothem growth did not cease completely during long periods of harsh climate conditions during the Beringen and Birrfeld glaciations and that permafrost terminating speleogenesis and speleothem growth was thus probably established only temporarily over relatively short periods. A conceptual model for the Middle Pleistocene to Holocene development of the Erdmannshöhle is presented within the framework of modern Quaternary lithostratigraphy. This model facilitates a first correlation of the cave evolution with the Middle to Late Pleistocene depositional record in the Möhlinerfeld, which is a key area for modern Quaternary lithostratigraphy in Switzerland and Southern Germany. Thus, speleological and Quaternary research, both based on a regional scale data compilation, complement one another with respect to the timing of events and the landscape evolution during the Quaternary and Late Neogene.

Keywords: Erdmannshöhle, Dinkelberg, Cave levels, U/Th dating, Pleistocene stratigraphy

1 Introduction

Caves are an almost perfect archive for the conservation of information concerning archaeology, palaeontology, hydrology, climate, tectonics and palaeoseismology. The main reason is that if a cave passage becomes inactive, cave sediments are protected against erosion and weathering for several thousands and up to millions of years. For decades, this favourable circumstance has allowed for the reconstruction of early human history by archaeological excavations, research on fossil remains by palaeontologists to reconstruct Pleistocene fauna (Schmidt et al.

2001), palynological investigations by botanists to reconstruct vegetation history (Quinif 2006), and more recent palaeo-climate research based on stable isotope analyses and various proxies in speleothems (Fairchild and Baker 2012). Additionally, neotectonic and speleoseismological research has been conducted to analyse tectonic displacements and earthquake-induced cave damage (Lemeille et al. 1999; Lignier and Desmet 2002). Based on progress in absolute age dating using the well-established radiocarbon and U/Th methods in addition to modern age dating methods with cosmogenic nuclides, it is now possible to accurately date a wide range of organic remains and sediments. These methods facilitate a correlation with Pleistocene deposits, in particular the glaciofluvial terraces in the large river valleys that form the base for the Pleistocene lithostratigraphy (Keller and Krays 2010, Preusser et al. 2011).

Editorial handling: Wilfried Winkler.

*Correspondence: arnfried.becker@gmail.com

¹ Max-Planck-Str. 6, 76351 Linkenheim-Hochstetten, Germany

Full list of author information is available at the end of the article



© The Author(s) 2020. This article is licensed under a Creative Commons Attribution 4.0 International License, which permits use, sharing, adaptation, distribution and reproduction in any medium or format, as long as you give appropriate credit to the original author(s) and the source, provide a link to the Creative Commons licence, and indicate if changes were made. The images or other third party material in this article are included in the article's Creative Commons licence, unless indicated otherwise in a credit line to the material. If material is not included in the article's Creative Commons licence and your intended use is not permitted by statutory regulation or exceeds the permitted use, you will need to obtain permission directly from the copyright holder. To view a copy of this licence, visit <http://creativecommons.org/licenses/by/4.0/>.

The Erdmannshöhle near Hasel at the NE margin of the Dinkelberg plateau, SW Germany, was discovered in 1754 while quarrying for Muschelkalk limestone. It has been a commercial cave since 1773, making it the second-oldest commercial cave in Germany (Siegener 1994). With a length of 2315 m (Siegener 1994), it is the longest cave in the Dinkelberg plateau. Over the last decades, new cave passages were discovered, and the cave was mapped by a local group of speleologists and geologically investigated in detail as part of a diploma thesis (Piepjohn 1987). A model for the evolution of the Erdmannshöhle was developed based on cave levels and allochthonous clastic cave deposits (Piepjohn 1987, 1995a; Piepjohn et al. 2005). However, without any absolute age datings, the age constraints were based solely on the links of the cave levels and the assumed ages of Pleistocene terraces in the Hasel valley.

In the following, we attempt to more precisely capture the formation and depositional history of the Erdmannshöhle in terms of absolute age and stratigraphy and present a detailed description of the cave evolution under regional constraints. This allows for the correlation of cave levels and cave deposits of the Erdmannshöhle with the terrace deposits in the Hochrhein valley, which is a key area for Pleistocene stratigraphy in Switzerland and Southern Germany (Penck and Brückner 1901-09, Hantke 1978-1983, Graf 2009). Finally, the potential of cave levels and cave sediments for Pleistocene stratigraphy is outlined.

2 Geological setting of the cave

2.1 Stratigraphy and tectonics

The Erdmannshöhle in SW Germany (Fig. 1) is located in a block-faulted area at the NE corner of the Dinkelberg plateau about 25 km NE of Basle. An overview of the area's stratigraphy is given in Table 1, starting with the crystalline basement rocks of the Black Forest, which are exposed at a distance of about 1000 m to the NE of the Erdmannshöhle (Fig. 1). Small remnants of Permian and Triassic red beds together with carbonates of the Lower and Middle Muschelkalk are exposed in the block-faulted area at the transition to the crystalline basement of the Black Forest (Lutz 1964; Piepjohn 1987). Middle Muschelkalk is also exposed in a small strip along the western slopes of the Hasel and Tunnelbach valleys (Fig. 1). Carbonates of the Upper Muschelkalk are most widespread on the surface, consisting predominantly of limestones at the base (Trochitenkalk), limestones with some marly intercalations at mid-section (Plattenkalk) and dolomites at the top (Trigonodus-Dolomit) (Table 1). They are covered by Keuper shales, marls and dolomites in a small graben to the NE (Fig. 1).

Close to the Erdmannshöhle gravel deposits are common (Fig. 1) and form terraces that are generally attributed to the Riss Glaciation (High Terrace) and the Würm Glaciation (Low Terrace) (Table 1) based on their degrees of weathering and topographic elevation (Lutz 1964, Piepjohn 1987, 1995b). Their ages are not constrained by absolute age dating. The base of the High Terrace E of the Hasel valley decreases from 440 m (a.s.l.) at Hummelberg in the N to 385 m W of Wehr in the S, and W of the Hasel valley from 430 m in the N to 395 m in the S (Fig. 2). The base of the Low Terrace decreases from 420 m N of Hasel to 380 m at the interface between the Tunnelbach and Hasel valleys in the S (Piepjohn 1995a) (Figs. 1, 2).

The area is characterized by N-S to NW-SE striking normal faults that show vertical offsets up to 50 m (Lutz 1964; Piepjohn 1987). The tectonically deepest section is reached in a small graben E of the Erdmannshöhle in front of the block-faulted transition zone to the crystalline basement of the Black Forest (Fig. 1). The layer dip is subhorizontal to a maximum of 10° to the W or SW in most parts of the area.

2.2 Karst environment

West of the fault following the Entengraben, the Tunnelbach valley and the Hasel valley the Muschelkalk forms a shallow open karst area with numerous dolines and streamless valleys on top of the relatively impermeable Middle Muschelkalk (Fig. 1). Several springs on top of the Middle Muschelkalk along the western slope of the Tunnelbach valley and the southern end of the Entengraben drain parts of the perched karst aquifer of the Dinkelberg plateau in the W (Fig. 1). These springs are all above the local drainage channel of the Hasel river.

The strip largely defined by the aforementioned fault and the western border fault of the small graben in the NE defines an open deep karst area with the relatively impermeable Middle Muschelkalk beds underneath. Dolines are numerous, as are collapse sinkholes in areas covered by Pleistocene gravels. Streamless valleys are the lower Wilsbach valley and the Entengraben. This area contains the Erdmannshöhle, the Pfarrhaushöhle in Hasel village and the Untere Wehrer Brunnenhöhle NW of Wehr (Fig. 1). The deep karst is fed by several ponors where the whole surface stream, or at least parts of it, disappear into the subsurface. Most important is the Schammernbach ponor in the NNW, which has recently been the most important feeder for the Erdmannshöhle cave stream (Figs. 1, 2). Further ponors are located in the Hasel valley, W of the Hummelberg and in the Wilsbach valley (Fig. 1). Based on tracer tests the subsurface flow paths between the different ponors and the resurgences

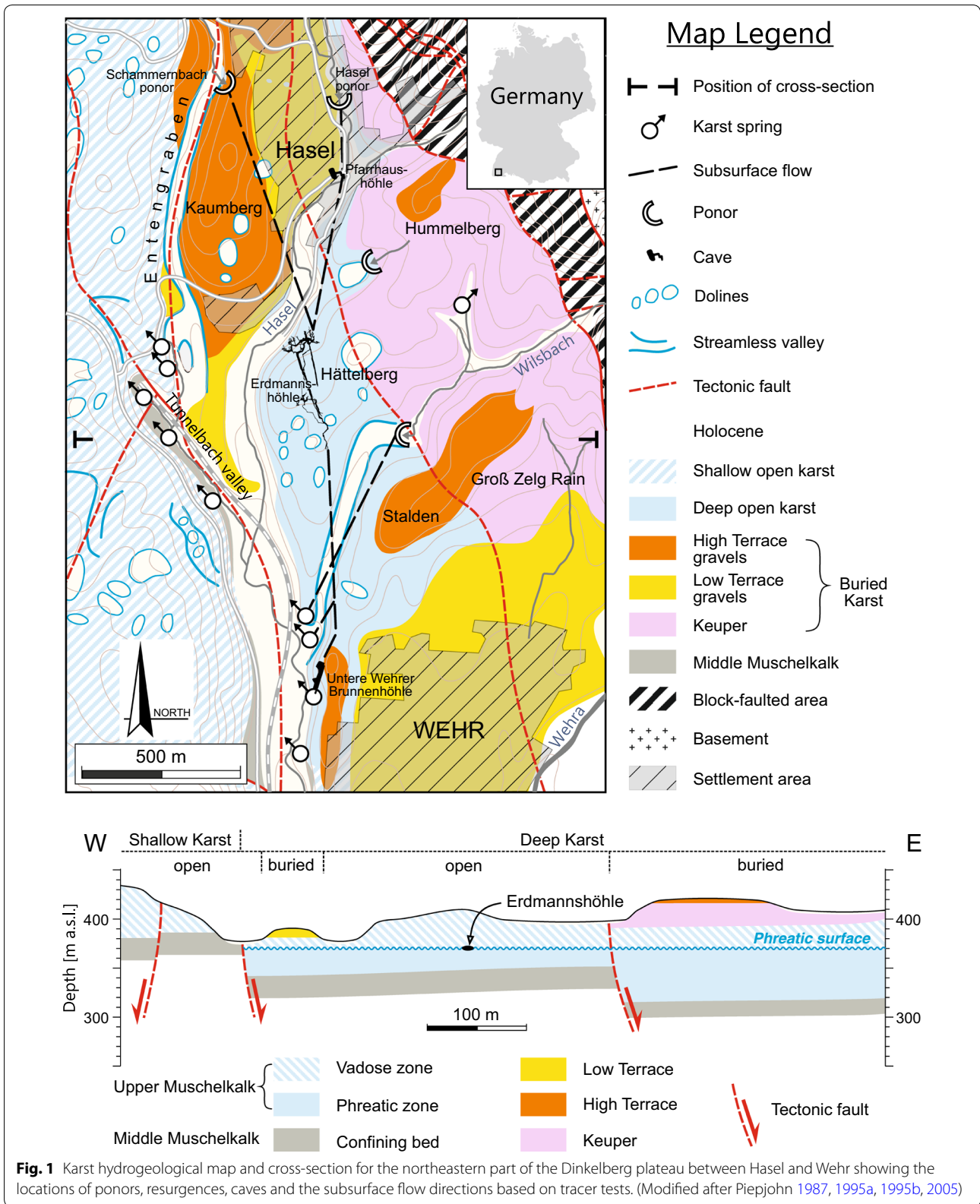


Table 1 Stratigraphic overview for the region of the Erdmannshöhle and comparison of the Pleistocene stratigraphic units used in Switzerland (used in this publication), Baden-Württemberg and Bavaria

Switzerland	Baden-Württemberg	Bavaria	Lithostratigraphy	Period
Holocene	Holocene	Holocene		Quaternary
Birrfeld	Würm	Würm	Low Terrace	
Eem	Eem	Riss/Würm		
Beringen/ Koblenz	Jung-Riss Doppelwall-Riss	Riss	Zeiningen Till	
Meikirch			High Terrace	
Hagenholz ? Habsburg	Älteres Riss ?			
Holstein	Holstein	Mindel/Riss		
Möhlín	Hosskirch	Mindel	Büntén Till	
Early Pleistocene			Deckenschotter	Triassic
			Keuper	
			Trigonodus-Dolomit	
			Plattenkalk	
			Trochitenkalk	
			Middle Muschelkalk	
			Lower Muschelkalk	
			Buntsandstein	
			Rotliegend	
			Crystalline basement	
				Permian
				Pre-Permian

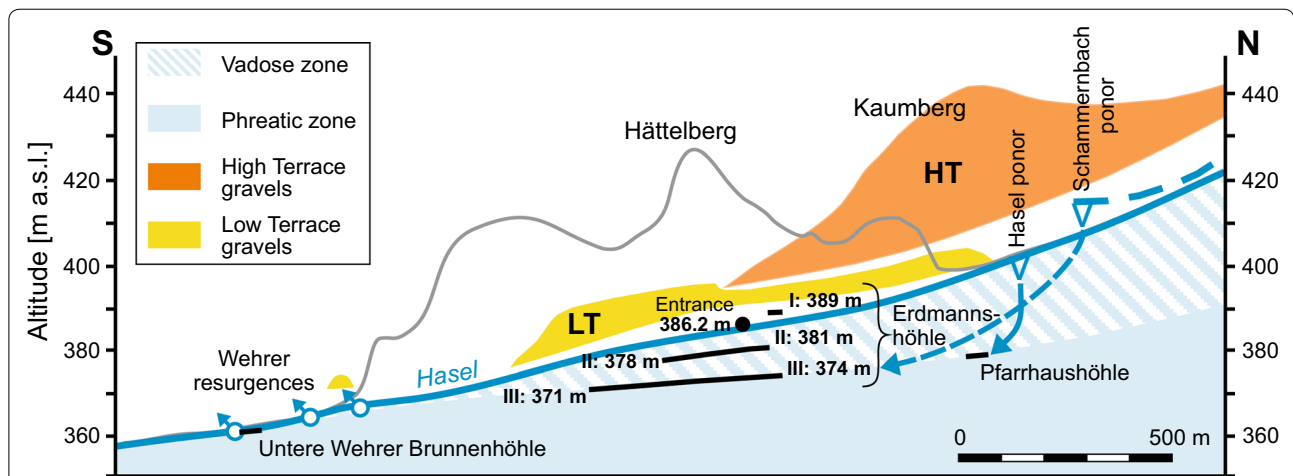


Fig. 2 Diagrammatic N-S profile along the Hasel valley with the altitudes of the base of the High and Low Terrace, the position of caves (Pfarrhaushöhle, Untere Wehrer Brunnenhöhle), the cave levels of the Erdmannshöhle (I-III) with their altitudes [m a.s.l.] and the karst hydrographic zones. (Modified after Piepjohn 1995a)

along the eastern Hasel valley W of Wehr could be detected. They are indicated by dashed lines in Fig. 1 (Piepjohn 1995a).

In the area occupied by the small graben in the NE, Upper Muschelkalk is covered by Keuper deposits, mainly shales, sandstones and thin dolomite beds. Nothing is known about the buried deep karst in this area.

3 The cave

3.1 Cave morphology and levels

The Erdmannshöhle developed along stratification crevasses in flat-lying, up to 10° W to SW dipping limestone, and along steep, NNW-SSE striking dominant joints (Piepjohn 1987) (Fig. 3). The control of fractures on the development of passages is clearly visible in the cave map, particularly for the Langer Gang, Verbindungsgang and the Oberer Bachgang with their long straight passages (Fig. 3). These passages follow 165°–175° striking, sub-vertical fractures (Piepjohn 1987), which drain the cave towards the S and SSE. The passage cross-sections are frequently box-shaped with flat ceilings and almost vertical side walls. This is common in thinly-bedded limestones in subcutaneous caves with a coverage from a few metres up to a few tens of metres (Filipponi 2003; Piepjohn et al. 2005; White 2005). Elliptical cross-sections are rarely seen, and, in connection with a canyon (“keyhole profile”), only developed in the Verbindungsgang and the Kapelle (Fig. 3). Cave collapse in the thinly-bedded limestones probably obliterated some of the initially elliptical cross-sections of cave passages. Besides the horizontal passages, shafts and dome pits of moderate dimensions formed (Fig. 4).

Small-scale solution features are rarely seen in the Erdmannshöhle. Scallop indicating a southward flow direction for the older cave levels are mentioned by Piepjohn (1987), which is in agreement with the recent flow direction in the Bachgang. Of interest are dissolution features in the ceiling of some cave passages that were once filled with sediments almost up to the ceiling. These dissolution grooves are well visible in the Labyrinth and the Eingangsgang (Fig. 3) and may point to paragensis.

Characteristic for the Erdmannshöhle are the cave levels (Figs. 2, 4) which are defined as groups of cave passages confined to a narrow vertical range. The conditions for the formation of cave levels are exemplarily achieved in the case of the Erdmannshöhle: (1) It is fed by two allogenic streams with uniform recharge due to high precipitation in their headwaters in the Black Forest mountains, (2) the surface waters completely (Schammernbach) or partly (Haselbach) seep into the subsurface, and (3) the groundwater flows through strongly fractured and gently dipping Muschelkalk limestone (Piepjohn 1987, 1995b; Piepjohn et al. 2005; Palmer 2007; Harmand

et al. 2017). Three main cave levels have evolved in the Erdmannshöhle. The top level I (around 389 m a.s.l.) is the shortest with respect to its lateral extent of accessible passages and is mainly represented by the Steffisgang and the Regenwald (Figs. 2, 3, 4). The intermediate cave level II (between about 381 and 378 m a.s.l.) is much larger and almost entirely occupied by the show cave. The Langer Gang, Irrgarten, Labyrinth, Fürstengruft, Rittersaal, Konferenzsaal and Dreikönig belong to cave level II (Figs. 3, 4). Cave level III is the youngest and has the largest extent. It can be subdivided into the temporarily flooded cave level IIIa (around 374 m a.s.l.), mainly represented by the Verbindungsgang, Lehmhölle and Troja (Fig. 3), and the active cave level III (between 374 and 371 m), which is occupied by the cave stream (Oberer and Unterer Bachgang). Between Oberer and Unterer Bachgang the only loop along the active cave level III is the 40-m-long siphon, which submerges 5–6 m below the level of cave level III (Piepjohn 1995a). Cave level III marks the top of the present-day karst water table. Shafts connect different cave levels, for instance the Brutaler Schacht between cave level II (Fürstengruft) and cave level IIIa (Lehmhölle) (Fig. 3).

3.2 Cave deposits

Fine-grained “cave loam” (clay and fine to medium silt) as well as fluvial sands and gravels of a cave stream are in most cases allochthonous deposits, whereas debris caused by cave collapse and speleothems resulting from precipitation of carbonates inside the cave are autochthonous deposits. Aside from cave collapse debris, all these sediments have the potential for absolute age dating: (1) “cave loam” for dating with OSL (optically stimulated luminescence) or radiocarbon of the organic content (e.g. bones, dispersed organic material), (2) sand and gravel for dating with OSL and cosmogenic nuclides, (3) speleothems for dating with U/Th, radiocarbon and ESR (electron spin resonance).

3.2.1 “Cave loam”

“Cave loam” is made up of clay and fine to medium silt. It is wet and sticky in cave level III/IIIa and fairly dry in cave level II (Figs. 3, 4). In the oldest cave level I, cave loam is not present. Cave loam is particularly enriched in the flood storage areas of cave level IIIa, i.e. Troja, Verbindungsgang and Lehmhölle (“loam hell”) (Fig. 3). In most cases, cave loam is an allochthonous sediment brought into the cave either with the cave stream by fluvial transport or washed into the cave along fissures and small karst conduits directly from the surface. Sub-surface erosion of marly and clayey intercalations in the Muschelkalk limestone is another possibility, but probably a minor source for cave loam.

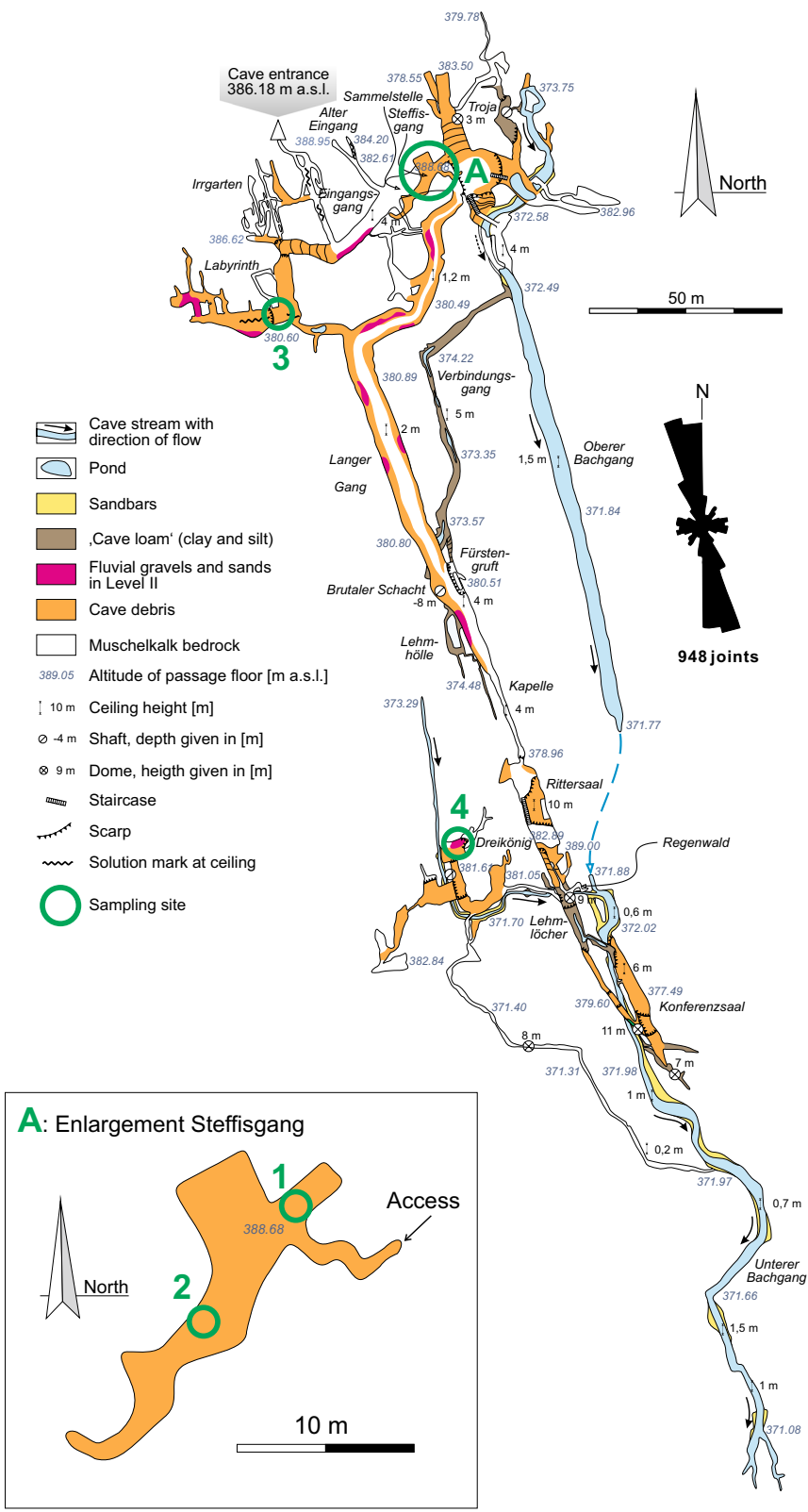
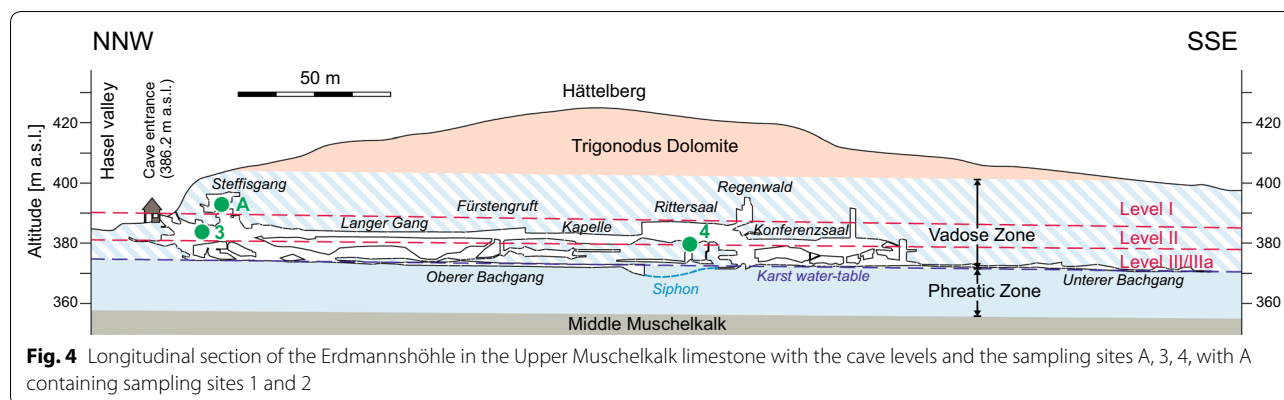


Fig. 3 Map of the Erdmannshöhle after Piepjohn (1987) and Piepjohn et al. (2005) with locations mentioned in the text and the sampling sites (1–4) for U/Th dating



3.2.2 Allochthonous gravels and sands

The allochthonous clastic sediments vary in size between coarse-grained silt and up to 25 cm large cobbles. They are built up of quartzites, granites and granodiorites from the crystalline basement of the Black Forest, arkoses and breccias from the Rotliegend, as well as some limestone and quartzite from the Muschelkalk, which is to some extent reworked cave collapse debris from within the cave. Besides the Bachgang in cave level III, which is still filled with more than 3 m of sediments (Piepjohn et al. 2005), allochthonous gravels and sands are only preserved as remnants. In cave level II, allochthonous sand and gravel deposits once filled cave passages almost up to the ceiling. This is particularly the case for some cave passages in the northern section of the Erdmannshöhle in cave level II, i.e. the Labyrinth, the Sammelstelle and the Langer Gang (Fig. 3). Here it looks as if most of the sediments were deposited under phreatic conditions, because cut-and-fill structures indicating open channel flow (Quinif 2006) are not documented. Also, upward solution in some cave passages in the northern part of the Erdmannshöhle originally filled by allochthonous siliciclastic sediments, i.e. the Alter Eingang, Eingangsgang and Labyrinth (Fig. 3), would support phreatic conditions, because paragenesis terminates at the water table (Palmer 2007; Harmand et al. 2017). In cave level I (Steffisgang) the allochthonous gravels and sands are already cemented and adhere at the cave walls as residues.

3.2.3 Cave collapse debris

Cave collapse debris is fairly common in the older cave levels I and II, but rarely seen in cave levels III/IIIa. It is a blocky debris of coarse-grained angular limestone fragments reaching sizes of up to several cubic metres in some cases. Depending on the age of the cave debris and the site of deposition, material is loose or cemented by sinter.

3.2.4 Speleothems

The Erdmannshöhle is rich in speleothems. Stalactites and stalagmites are particularly common in cave levels I and II, and some of them are fairly large. Surprisingly, the deepest and still active cave levels III/IIIa in the Erdmannshöhle also show some large speleothems (Piepjohn 1987). In the Verbindungsgang (cave level IIIa), these include the 4.5 m tall stalagmite called “Der Einsame” (Siegener 1994), and, in the active Bachgang (cave level III), the stalactite called “Der Grosse” (Siegener 1994). The latter is about 3 m long and widens towards the tip, terminating about 20 cm above the normal runoff water level of the cave stream. Flowstone is fairly common in cave level II, particularly in the Langer Gang and the Dreikönig, but is rarely seen in other parts of the Erdmannshöhle.

4 U/Th dating

Absolute age dating is important for stratigraphy, palaeoclimate studies and the precise correlation of climatic events documented in cave deposits (e.g. Cheng et al. 2009; Fleitmann and Matter 2009; Griffiths et al. 2010; Zhao et al. 2010; Spötl and Cheng 2014, Spötl and Boch 2019). It is also extremely helpful and necessary for archaeological reconstructions (e.g. Wenz et al. 2016; Hoffmann et al. 2018).

Uranium–thorium disequilibrium dating is the most commonly used method for the absolute dating of cave deposits (Fairchild and Baker 2012). The hypothesis of a closed system is required for the application of uranium/thorium disequilibrium to cave carbonates. Calcite incorporates uranium when it crystallises (uranium is water-soluble, but thorium is not). At the time of crystallisation, the meter is set to zero. With time, ^{230}Th begins to appear due to the decay of ^{234}U , and the activity ratio of both elements can be used to determine the time elapsed since the calcite deposit (Sauvet et al. 2017). The rapid technical development in the field of mass spectrometry allows

high-precision age determination in the epsilon range for sample quantities in the mg range (Arps 2017) and is the single most important factor that has allowed speleothem science to become so prominent in recent years (Fairchild and Baker 2012).

4.1 Sampling sites

Samples for U/Th dating were taken from two sites in the Steffisgang (A1, A2 in Fig. 3) which is part of the uppermost and oldest cave level I (A in Fig. 4), and from two sites in the intermediate level II, one each from the Labyrinth and Dreikönig (3 and 4 in Figs. 3, 4). Views of the sample sites are shown in Fig. 5.

4.1.1 Steffisgang

The first sample was taken from cave debris immediately behind the narrow entrance of the Steffisgang (A1 in Figs. 3, 5a). The stalagmite was part of a thin flowstone layer that grew on a small debris cone deposited on top of a Muschelkalk limestone bench. The bench failed and toppled, reversing the upper surface by about 120° (Fig. 5a). The stalagmite is 20–60 mm high with a diameter of about 50 mm. The coarse-grained angular limestone debris at the base of the stalagmite is cemented by sinter (Fig. 6a). A thin layer directly at the base of the stalagmite shows fine-grained subangular to well-rounded allochthonous components, mainly quartzite and granitoids. The stalagmite is laminated, showing some minor contamination by two brownish layers near the base. The sinter is dark grey at the centre and becomes brighter towards the periphery. Two samples defining the period of stalagmite growth were taken for U/Th dating, one near the base (Sample ID: 9538), and the other close to the surface (ID: 9537) (Fig. 6a, Table 2).

The second sample taken in the Steffisgang (A2 in Fig. 3) is a small stalactite, 210 mm long and 27 mm in diameter, which rested on top of a thin layer of coarse-grained cave debris in the immediate vicinity of the stalagmite shown in Fig. 5b. The stalactite was broken into two pieces and strongly etched along one side so that the central tubular canal came close to the surface (Fig. 5c). From the other largely unetched side, two samples for U/Th dating have been taken close to the root of the concentrically layered stalactite, one directly near the central canal (9268) and one closer to the periphery (9269) (Fig. 6b, Table 2).

The third sample from the same location (A2 in Figs. 3, 5b) is an in situ stalagmite that grew on solid rock and was covered by loose blocky limestone debris. It consists of a group of three coalesced stalagmites. The largest stalagmite is 110 mm high with a diameter between 60 and 110 mm, the intermediate one is 90 mm high with a

diameter of 60 mm, and the smallest is 70 mm high with a diameter of 40 mm.

Because of the shape of the large stalagmite with its flat top, it looked at a first glance like a stalagmite stump (Fig. 5b). However, in two sections cut perpendicular to each other, the top of the large stalagmite looks as if some dissolution took place at the surface causing the stump-like morphology (Fig. 7). The internal layering is well visible in the saw cut parallel to the growth direction, which shows three sections of slightly brownish layering probably caused by some argillaceous contamination. The longitudinal section parallel to the growth direction suggests a movement of the drip source as indicated by the stalagmite layering with very thin layers near the exposed oblique surface and the thick layers at the opposite side. Two samples were taken close to the base (9386) and the top (9387) of the stalagmite (Fig. 7b, Table 2).

The intermediate stalagmite is partly covered by the large stalagmite (Fig. 7a), indicating that it is older than the large stalagmite. Laminated brownish layers halfway up the intermediate stalagmite indicate a growth anomaly separating a light to medium grey core from a medium and partly dark grey top-section. Samples were taken from the core close to the base (9384) and from the top (9385) of the intermediate stalagmite (Fig. 7a, Table 2).

4.1.2 Labyrinth

A small sinter column was taken for sampling from the Labyrinth (3 in Fig. 3, Fig. 5d). The whole column was hanging from the cave ceiling with the bottom of the column 1.86 m above the modern cave floor (Fig. 5d), indicating significant erosion since the growth of the sinter column. The sinter column is about 350 mm high, 300 mm wide and 200 mm deep and consists of at least five small stalagmites and three stalactites and some relics of a former flowstone with interbedded allochthonous clastic sediments (bordered by a yellow line in Fig. 8). Samples were taken from the flowstone surrounding nests of siliciclastic intercalations (8790, 8792, 8793) as well as near the base (8949, 8789) and the top (8948) of one stalagmite (Fig. 8, Table 2).

4.1.3 Dreikönig

From Dreikönig in cave level II, two samples from a flowstone were taken for U/Th dating, one from the cave debris (Fig. 9a) and one cored from an in situ flowstone resting on top of fluvial gravels (4 in Figs. 3, 4 and Figs. 5e, 9b). The flowstone samples were finely laminated with some sand grains attached at the base and with some thin sandy intercalations within the flowstone. Samples for U/Th dating from flowstone

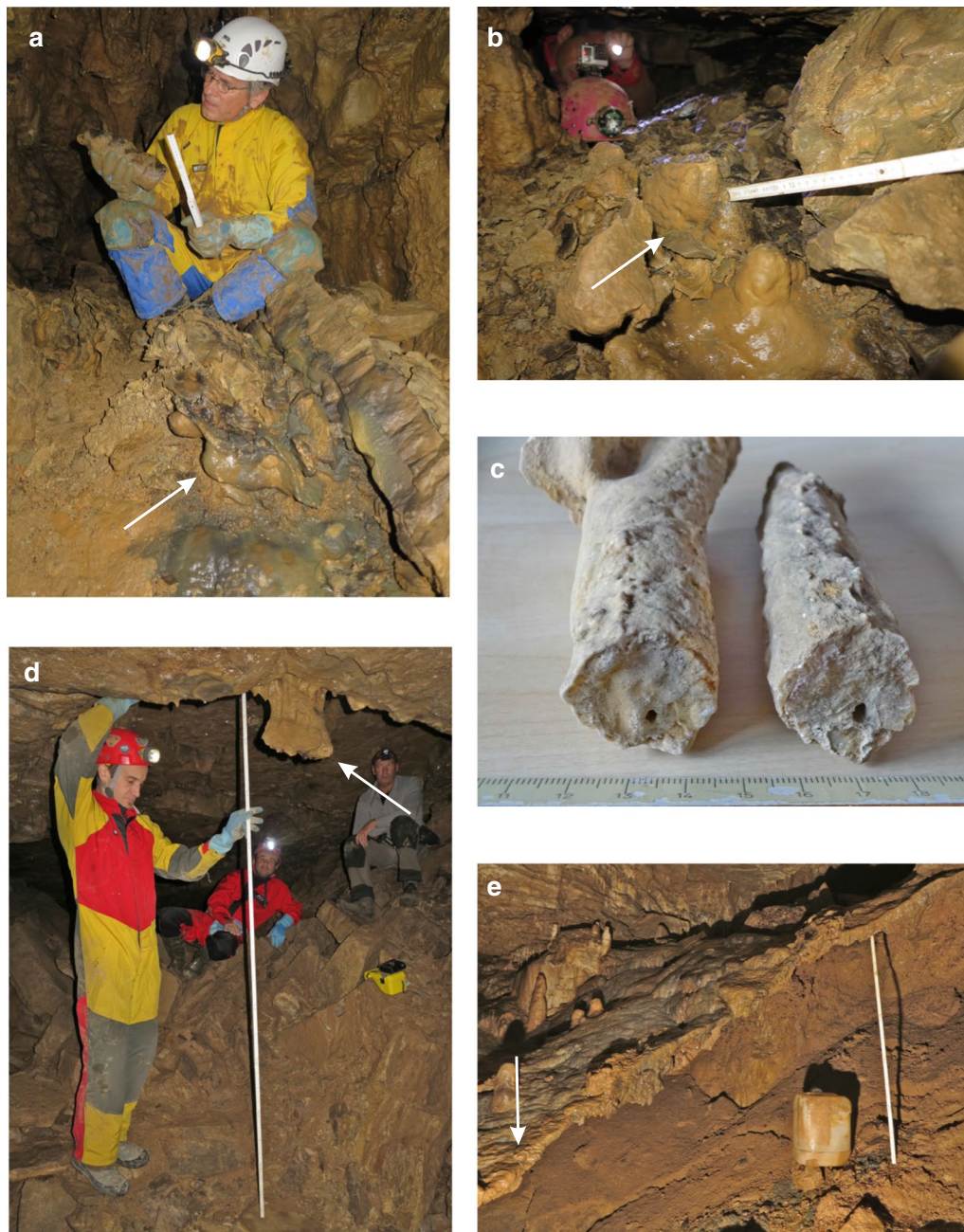


Fig. 5 Sampling sites for U/Th dating. **a** Site 1 in Steffisgang (cave level I) with small stalagmite (arrow) on debris and on top of a failed Muschelkalk bench. **b** Site 2 in Steffisgang with the in situ stalagmite. From the same site 2, the small stalactite was also sampled as shown in **(c)**. **d** Site 3 in the Labyrinth in cave level II with the position of the small sinter column at the ceiling (arrow) 1.86 m above ground (scale: 2 m). **e** Site 4 in Dreikönig. The samples were taken from the flowstone on top of the gravel deposit (scale: 1 m)

layers on top of the underlying siliciclastic deposits (8564, 8565, 8794, 8795) (Fig. 9, Table 2) post-date the deposition of the fluvial cave sediments.

4.2 Sample treatment and dating

Stalagmites, flowstone and stalactite were cut and samples of approx. 200 mg for $^{230}\text{Th}/\text{U}$ -dating were taken perpendicular to the growth axis, generally at the base and the top of the speleothem. Sample preparation for $^{230}\text{Th}/\text{U}$ -analysis was performed at the



Fig. 6 Sections of the stalagmite from site 1 (a) and the stalactite from site 2 (b), both from Steffisgang (cave level I) with the position of the samples taken for U/Th dating (numbers refer to the sample code in Table 2). Scale in centimetres

Institute of Environmental Physics, Heidelberg University, Germany. The samples were cut with a band saw. The carbonate slabs, weighing approx. 200 mg were mechanically cleaned and leached with weak nitric acid. The chemical procedure involving the ion-chromatographic separation of uranium and thorium from calcium carbonate using Eichrom UTEVA resin was carried out in an ultra-clean laboratory. The methods for sample preparation and mass spectrometric analysis follow the procedure of Douville et al. (2010); Matos et al. (2015); Arps (2017) and Wefing et al. (2017). Activity ratios were analysed with a Thermo Fisher Neptune MC-ICPMS at the Institute of Environmental Physics, Heidelberg University, Germany. The calibration of the ^{233}U , ^{236}U and ^{229}Th spikes used is described in Hoffmann et al. (2007). Replicated measurements of the HU-1 standard yield a reproducibility of the activity ratios of ($^{234}\text{U}/^{238}\text{U}$) of 1.00002 ± 0.00082 and for ($^{230}\text{Th}/^{238}\text{U}$) 1.0004 ± 0.0018 (Wefing et al. 2017). Blanks are smaller than 0.4 fg for ^{234}U and 0.04 fg for ^{230}Th . Ages were calculated using the half-lives of Cheng et al. (2000). Correction for detrital contamination assumes a $^{232}\text{Th}/^{238}\text{U}$ weight ratio of 3.8 ± 1.9 and

^{230}Th , ^{234}U and ^{238}U in secular equilibrium. Age uncertainties are quoted at the 2σ -level and do not include half-life uncertainties.

In total, 18 samples were analysed for uranium-series dating. The three samples 8790, 8792 and 8793 (Fig. 8) from the sinter column of the Labyrinth (3 in Figs. 3, 4 and Fig. 5d) showed extremely high thorium concentrations. Due to the Th correction thus required, age uncertainty increased to greater than ± 11000 years. These samples are presented in Table 2 and, though generally fitting into the picture, are not considered further due to the high age uncertainties.

4.3 Results

The most reliable U/Th dating results listed in Table 2 are illustrated in Fig. 10 together with the Marine Isotope Stages [MIS] (Martinson et al. 1987; Lisiecki and Raymo 2005) and the Middle to Late Pleistocene lithostratigraphy (Keller and Krayss 2010, Preusser et al. 2011).

In Dreikönig U/Th dating indicates flowstone growth during MIS 2, which corresponds to the Late Glacial Maximum including the main advance of glaciers in the Swiss Alpine foreland during the Birrfeld

Table 2 Results of the U/Th dating on speleothem samples from the Erdmannshöhle

IUP ID	Sample	^{238}U (ng/g)	^{232}Th (ng/g)	$^{230}\text{Th}/^{238}\text{U}^a$	$^{230}\text{Th}/^{232}\text{Th}^a$	$\delta^{234}\text{U}$ (‰)	Age (ka)	Age _{corr.} (ka)	$\delta^{234}\text{U}_{\text{initial}}$ (‰)
Fig. 9a									
IUP-8564	Dreikönig Test sample	506.389 ± 0.028	37.697 ± 0.087	0.32100 ± 0.00084	13.106 ± 0.046	402.33 ± 0.78	28.027 ± 0.083	26.63 ± 0.71	433.8 ± 1.2
IUP-8565	Dreikönig Test sample	586.546 ± 0.032	13.133 ± 0.037	0.2751 ± 0.0010	37.35 ± 0.17	301.85 ± 0.89	25.680 ± 0.094	25.23 ± 0.27	324.2 ± 1.0
Fig. 9b									
IUP-8794	Dreikönig Drill core	168.961 ± 0.015	76.92 ± 0.16	0.3217 ± 0.0015	2.148 ± 0.011	1033.2 ± 5.1	18.539 ± 0.093	12.5 ± 2.9	1070 ± 10
IUP-8795	Dreikönig Drill core	198.233 ± 0.017	39.042 ± 0.070	0.2569 ± 0.0010	4.018 ± 0.017	994.3 ± 3.1	14.890 ± 0.070	12.3 ± 1.4	1029.4 ± 5.1
Fig. 8									
IUP-8789 a	Labyrinth Stalagmite	501.610 ± 0.045	38.699 ± 0.059	0.7982 ± 0.0013	31.697 ± 0.071	306.0 ± 2.1	98.24 ± 0.37	96.76 ± 0.84	402.2 ± 2.9
IUP-8789 b	Labyrinth Stalagmite	511.491 ± 0.039	128.93 ± 0.22	0.8210 ± 0.0017	9.916 ± 0.027	300.9 ± 1.6	103.38 ± 0.41	98.4 ± 2.5	397.4 ± 3.5
IUP-8790 a	Labyrinth Flowstone	616.463 ± 0.073	180.41 ± 3.6	1.0157 ± 0.0032	1.0579 ± 0.0040	412.5 ± 3.2	126.68 ± 0.79	57 ± 40 ^b	485 ± 55
IUP-8790 b	Labyrinth Flowstone	450.574 ± 0.047	75.11 ± 1.3	0.9870 ± 0.0024	1.8175 ± 0.0054	427.5 ± 3.4	118.20 ± 0.64	85 ± 21 ^b	544 ± 33
IUP-8792 a	Labyrinth Flowstone	495.862 ± 0.050	94.66 ± 1.6	0.9505 ± 0.0024	1.5145 ± 0.0046	335.2 ± 2.1	125.86 ± 0.56	83 ± 24 ^b	424 ± 29
IUP-8792 b	Labyrinth Flowstone	431.017 ± 0.044	397.61 ± 0.78	0.8604 ± 0.0021	2.8691 ± 0.0090	298.4 ± 2.5	111.95 ± 0.65	93 ± 11 ^b	388 ± 13
IUP-8793	Labyrinth Flowstone	526.288 ± 0.052	800.3 ± 1.9	0.9603 ± 0.0026	1.9168 ± 0.0069	297.5 ± 2.2	135.92 ± 0.87	103 ± 21 ^b	398 ± 24
IUP-8948	Labyrinth Stalagmite	410.948 ± 0.026	98.29 ± 0.17	0.7592 ± 0.0019	9.773 ± 0.030	228.2 ± 2.1	100.96 ± 0.55	95.9 ± 2.5	299.3 ± 3.4
IUP-8949	Labyrinth Stalagmite	558.960 ± 0.036	23.242 ± 0.050	0.8396 ± 0.0022	62.09 ± 0.21	343.6 ± 1.7	101.26 ± 0.46	100.49 ± 0.61	456.4 ± 2.4
Fig. 7a									
IUP-9384	Steffisgang Stalagmite	791.995 ± 0.071	10.170 ± 0.017	0.9342 ± 0.0015	223.32 ± 0.52	172.08 ± 0.61	162.53 ± 0.63	162.25 ± 0.66	272.2 ± 1.1
IUP-9385	Steffisgang Stalagmite	410.143 ± 0.026	7.804 ± 0.013	0.7754 ± 0.0014	124.98 ± 0.30	167.43 ± 0.75	114.76 ± 0.39	114.34 ± 0.43	231.3 ± 1.1
Fig. 7b									
IUP-9386	Steffisgang Stalagmite	563.965 ± 0.024	7.295 ± 0.013	0.7400 ± 0.0014	175.64 ± 0.45	118.62 ± 0.44	115.02 ± 0.38	114.72 ± 0.40	164.05 ± 0.64
IUP-9387	Steffisgang Stalagmite	377.069 ± 0.019	3.2029 ± 0.0063	0.7682 ± 0.0021	277.81 ± 0.93	203.1 ± 1.2	106.77 ± 0.51	106.60 ± 0.52	274.4 ± 1.7
Fig. 6a									
IUP-9537	Steffisgang Stalagmite	477.023 ± 0.027	1.0534 ± 0.0023	1.0770 ± 0.0026	1497.4 ± 4.9	611.6 ± 1.2	109.74 ± 0.41	109.71 ± 0.45	833.9 ± 1.9
IUP-9538	Steffisgang Stalagmite	496.80 ± 0.15	8.091 ± 0.023	1.0291 ± 0.0032	194.08 ± 0.82	539.9 ± 1.6	110.45 ± 0.52	110.20 ± 0.64	737.1 ± 2.6
Fig. 6b									
IUP-9268	Stalactite	1067.504 ± 0.042	51.510 ± 0.062	0.8940 ± 0.0013	56.87 ± 0.11	132.45 ± 0.65	161.19 ± 0.48	160.11 ± 0.79	208.3 ± 1.1
IUP-9269	Stalactite	650.570 ± 0.029	122.59 ± 0.17	0.9270 ± 0.0019	15.090 ± 0.037	248.62 ± 0.94	138.03 ± 0.58	134.3 ± 1.9	363.4 ± 2.4

^a Activity ratios; _{corr.} corrected for detrital Th with $^{232}\text{Th}/^{238}\text{U}$ weight ratio of 3.8 ± 1.9 and ^{234}U , ^{238}U and ^{230}Th in secular equilibrium; 1ka = 1000 years; all measurements performed with a ThermoFischer Neptune Plus MC-ICP MS; errors 2 σ ; ^bages not shown in Fig. 10

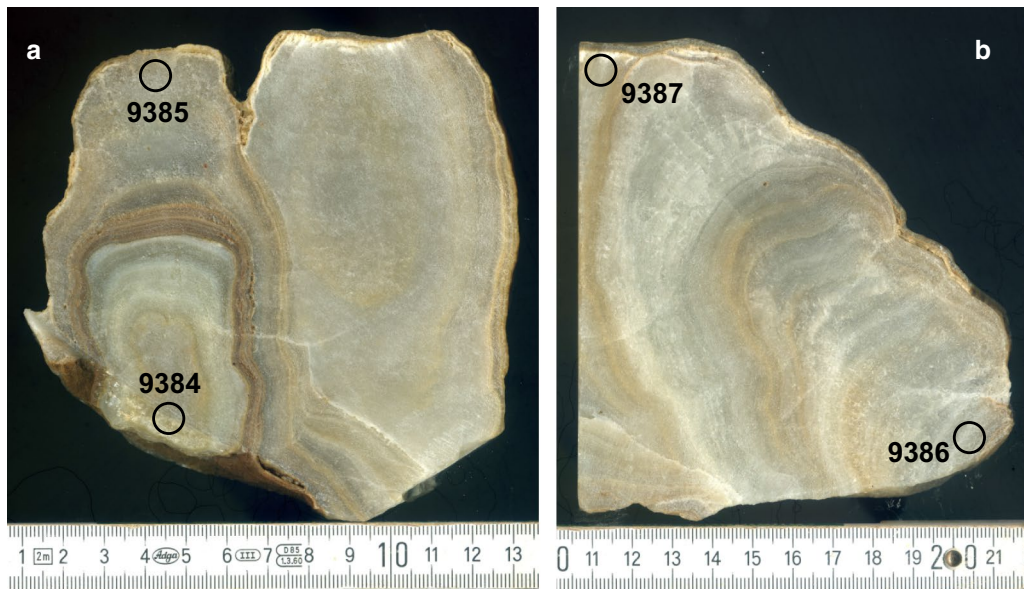


Fig. 7 Sections of the group of small stalagmites from site 2 in Steffisgang, cave level I. **a** section through the intermediate stalagmite and the large stalagmite (right) perpendicular to the growth direction, **b** section through the large stalagmite parallel to the growth direction. Positions of U/Th samples with the sample codes (cf. Table 2) are indicated. Scale in centimetres

Glaciation between 22 and 24 ka (Keller and Krays 2010). The samples 8564 and 8565 (Table 2) with ages of 26.631 ± 0.71 ka and 25.23 ± 0.27 ka just predate the main advance, whereas the samples 8794 and 8795

(Table 2) showing ages of 12.5 ± 2.9 ka and 12.3 ± 1.4 ka are within the Younger Dryas Stadial at the end of the Pleistocene. The samples dated were taken immediately on top of the allochthonous cave deposits indicating the initiation of flowstone growth in a very cold periglacial climate. This is somehow surprising, because one would expect deep-seated permafrost to a depth in the order of 150 m in the area not covered by glaciers (Delisle et al. 2003; Haerberli 2010; Govaerts et al. 2016), which would prevent karstification and speleothem growth. However, the results of U/Th dating in the Dreikönig point to much shorter periods of permafrost than so far assumed. Similar observations are reported from the Swabian Alb from the Hintere Kohlhalden Cave (21.0 ± 0.9 ka) and the Arbeitslosen Cave (21.1 ± 4.3 ka) (Kempe et al. 2002; Abel 2003).

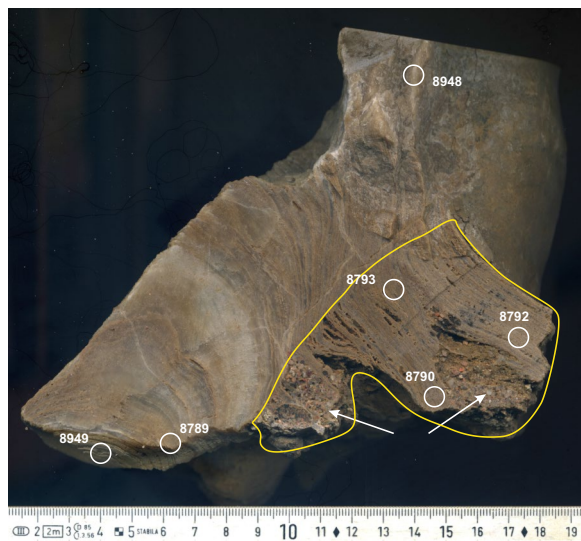


Fig. 8 Section through the sinter column from site 3, Labyrinth, cave level II. Indicated by a yellow line is the flowstone relict including nests of allochthonous siliciclastic sediments. To the left of the flowstone is a stalagmite at the base passing over into a stalactite at the top. Positions of U/Th samples with the sample codes (cf. Table 2) are indicated. Scale in centimetres

Flowstone remnants attached to the sinter column taken from the Labyrinth contain inclusions of allochthonous clastic sediments (Fig. 8). Obviously, sedimentation of some clastic sediments still took place during flowstone growth. Using flowstone samples from between the clastic inclusions may allow direct dating of the final stages of allochthonous clastic sedimentation in this part of the cave. Although the ages of the samples (8790, 8792, 8793) generally fit the ages of the samples taken directly from the sinter column, the high contamination with detrital thorium led to high age uncertainties. The U/Th dates from samples taken near the base and top of the sinter column provided much more reliable results

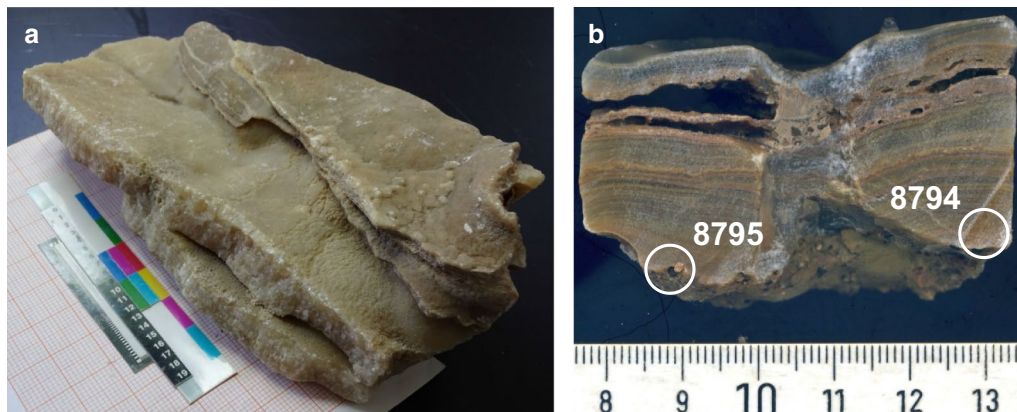


Fig. 9 Samples from site 4 (cf. Figs. 3, 4), Dreikönig, cave level II. **a** two U/Th samples (8564, 8565 in Table 2) were taken from the base of the specimen, **b** small drill core with a diameter of 6 cm from flowstone (cf. arrow in Fig. 5e) with position of U/Th samples (8794, 8795) at the base of the drill core

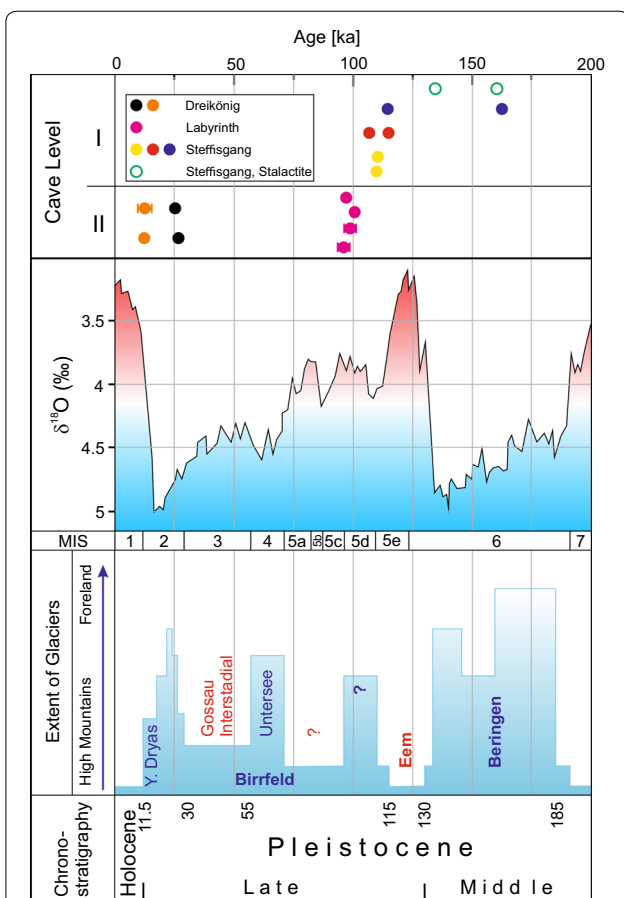


Fig. 10 Age of the U/Th samples in the cave levels I and II of the Erdmannshöhle with error bars in case of dating error greater than 2.5 ka compared to the $\delta^{18}O$ values and the MIS stages after Lisiecki and Raymo (2005) and the Quaternary lithostratigraphy for Switzerland after Graf (2009), Keller and Krays (2010) and Preusser et al. (2011) [cf. Figure 11]

(8789, 8949, 8948 in Table 2, Fig. 8). They indicate growth of the sinter column during the early Birrfeld Glaciation between 100.5 and 95.9 ka in late MIS 5d and early MIS 5c.

U/Th dating on samples from the Steffisgang (cave level I) mainly indicate an Eem Interglacial age, although in some cases speleothem growth was already initiated during the Beringen Glaciation (Fig. 10). The oldest stalagmite is the intermediate stalagmite (Fig. 7a) at site A2 in Fig. 3. The base sample of this stalagmite (9384) gives an age of 162.25 ± 0.66 ka (Table 2), which indicates onset of stalagmite growth in the middle of the Beringen Glaciation [MIS 6] (Fig. 10). However, halfway up the stalagmite a growth anomaly shows a marked brown layer rich in clay. This event could well correlate with the main advance of the Wehratal glacier, which demonstrably reached the Hochrhein valley during the Beringen Glaciation (Graf 2009; Preusser et al. 2011). The stalagmite stopped growing at 114.34 ± 0.43 ka during the late Eem Interglacial [MIS 5e]. The intermediate stalagmite took about 48 ka to reach a height of 90 mm, i.e. a growth rate < 2 mm/ka. This small growth rate is probably related to a lengthy interruption of stalagmite growth during the Beringen Glaciation. Just when the intermediate stalagmite stopped growing, the nearby large stalagmite started to grow (sample 9386 in Table 2, Fig. 7b). Compared to the intermediate stalagmite the large one grew relatively fast within 8 ka (114.7–106.6 ka) during the late Eem Interglacial and early Birrfeld Glaciation (MIS 5e/5d) (Fig. 10) and did not show any significant growth anomalies. The oblique growth direction is not due to tilting of the stalagmite but probably to the shift of the drip point at the ceiling of the cave.

At about the same time as the Eem Interglacial ended, the small stalagmite from site A1 in Fig. 3 grew in a very short time span between 110.20 ± 0.64 ka and 109.71 ± 0.45 ka, as indicated by the two samples 9538 and 9537 (Fig. 6a, Table 2). The only stalactite taken for U/Th dating is from site A2 in Fig. 3. Because of the very fine layering of the stalactite, the ages listed in Table 2 are “mixing ages” across several laminae. Sample 9268 gives an age of 160.11 ± 0.79 ka (Table 2), which is very close to the onset of growth of the intermediate stalagmite at site A2 (Fig. 3) in the middle Beringen Glaciation [MIS 6] (Fig. 10), whereas the outer sample 9269 (134.3 ± 1.9 ka) still shows some growth near the end of the Beringen Glaciation. The stalactite probably stopped growing during the Eem Interglacial.

5 Some basic aspects of cave formation

5.1 Minimum time span for cave passage development

Open space that allows dissolving groundwater to penetrate and pass through carbonate bedrocks is a precondition for karstification. Karst conduits may then develop in four stages: (1) pre-breakthrough laminar flow in narrow voids, preferably joints and bedding planes with a threshold diameter of at least $10\text{--}25$ μm (Böcker 1969; Dreybrodt 1988; White 1988); (2) post-breakthrough turbulent flow uniformly enlarging the conduit under phreatic conditions, (3) possibly vadose entrenching, and finally (4) initiation of its decay after the water abandons the passage. Short direct flow paths with low flow resistivity and towards the largest hydraulic gradient are most likely to attract the greatest flow. Fractures meet this condition best.

The initial stage up to the breakthrough strongly depends on the initial width of the voids in addition to the parameters p_{CO_2} and temperature. This stage may last for 1000 and up to 10 million years (Palmer 1991; Dreybrodt and Gabrovšek 2000; Faulkner 2006). However, in case of the Erdmannshöhle with (1) its close sequence of cave levels where fractures may already have passed the breakthrough stage at depth before valley incision readjusted the karst aquifer to a deeper discharge level, and which (2) developed most of the time under boreal or periglacial conditions, and (3) with ponors less than 1000 m S of crystalline basement rocks of the Black Forest which are a source for aluminosilicates that reduce the reaction rate with the carbonate bedrock and increase the penetration length of the less saturated solution (Faulkner 2006), the period up to the breakthrough probably comes closer to 1000 years instead of several million years.

After breakthrough, the enlargement of the conduit proceeds under phreatic conditions at a rate of about 0.2 mm/a, which is similar for all phreatic conduits

independent of their former development (Dreybrodt and Gabrovšek 2000) and largely depends on the amount of water that can be attracted by and pass through the conduit. Passage enlargement may even be greater for the Erdmannshöhle with low hardness recharge from crystalline basement catchment areas. For alpine conditions with high flow rates and unsaturated solutions, wall retreat rates are in the range of 0.05–1.0 mm/a (Faulkner 2006). These values suggest that a traversable cave passage can easily form in about 10,000 years (Palmer 2000). If the water table drops, the conduit becomes vadose with a stream flowing in it. Entrenching of a canyon may occur at similar rates until the conduit falls dry.

Applying an enlargement rate of 0.2 mm/a applied to the cave passages of the Erdmannshöhle, the following time for their formation can be estimated: in cave level II the Rittersaal and Langer Gang with widths in the order of 6.2 m each as taken from the cave map (Fig. 3) would yield a time span of about 31 ka for their formation, the Labyrinth with a width of 4.6 m and the Sammelstelle with a width of 4.1 m about 20–23 ka; in cave level IIIa the Verbindungsgang showing a width between 1.0 and 2.6 m would form in about 5–13 ka, and in cave level III, the active Bachgang with a width of 3.9 m in about 19 ka. In summary, for most cave passages in the Erdmannshöhle the time span for their formation after the breakthrough is in the order of 20–30 ka.

5.2 Development of cave levels

Cave levels are related to base levels in nearby river valleys and develop when an entrenching river experiences a long period of almost static base level (Palmer 2007; Audra and Palmer 2011). Then, springs fed by the karst aquifer tend to remain stable over long time periods without shifting elevation, and cave passages remain active long enough to grow by solution. Only phreatic passages with low hydraulic gradient and uniform recharge in bedrock can form true cave levels near the top of the karst water table (Palmer 2007; Harmand et al. 2017). Such water table caves without or rare loops are particularly common in flat-lying or gently dipping, intensively fractured strata (Ford and Ewers 1978). On the other hand, rapid and significant valley incision causes the karst aquifer to readjust to a deeper discharge level. Cave passages at the former river level quickly fall dry or develop entrenched canyons in their floors. Base-level lowering is common in most temperate climate karstic areas due to uplift of the crust and associated valley incision. Combined with surface data—erosional benches, cut-terraces, alluvial terraces—cave levels can provide information about the local erosional and depositional history (Abel et al. 2002; Harmand et al. 2017).

5.3 Timing of allochthonous siliciclastic sand and gravel deposition

In Europe, the aggradation of allochthonous siliciclastic sediments mainly occurred during cold periods and culminated during deglaciation in massive deposition of gravel and sand, whereas major incision primarily occurs during cold-to-warm transition when glacial sediment sources are depleted and the melt water discharge is still high (Bridgland and Westaway 2007; Graf 2009; Claude et al. 2017). Based on palynostratigraphical investigations as well as on age dating of speleothems and allochthonous clastic sediments in several caves in France, Belgium, Germany and Switzerland, this seems to also hold true for allochthonous clastic sediments in caves. It can be generally concluded that such clastic sediments in caves are mainly deposited during cold glacial periods due to intense mechanical weathering and soil erosion in a deforested barren landscape. In contrast, speleothem growth and erosion of allochthonous cave deposits due to base-level fall of the discharge system primarily

occurs during warm interglacial periods (Abel et al. 2002; Häuselmann 2002; Kempe et al. 2002; Abel 2003; Quinif 2006; Harmand et al. 2017). Thus, the glaciofluvial terraces in the Hasel valley and adjacent hill-sites (Figs. 1, 2) could easily be the main source for the allochthonous sand and gravel deposits in the different cave levels of the Erdmannshöhle.

5.4 Speleothem growth rates

Speleothem growth under phreatic conditions is usually impossible. It generally commences after the ceiling or the floor of the cave emerge from the karst water table. Speleothems primarily grow during warm interglacial or interstadial periods with rich vegetation and soil causing intense chemical weathering at the surface and carbonate precipitation due to CO₂ degassing in the cave. Growth rates for stalagmites in the Erdmannshöhle can be roughly estimated based on U/Th dating carried out in the cave levels I (Steffisgang) and II (Labyrinth). Taking only those stalagmites that

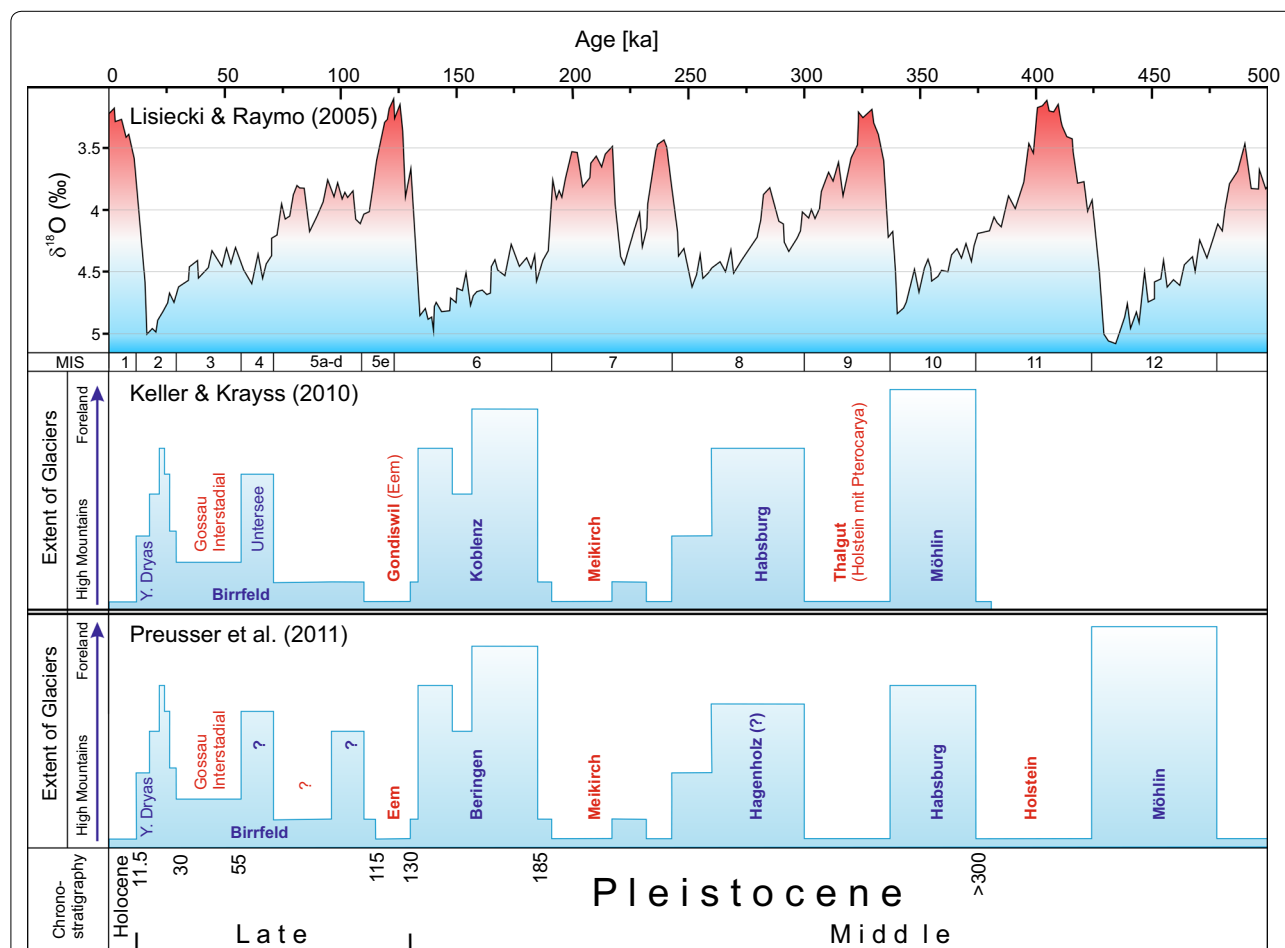


Fig. 11 Quaternary lithostratigraphy after Keller and Krays (2010) and Preusser et al. (2011) in comparison with the $\delta^{18}\text{O}$ values and MIS stages after Lisiecki and Raymo (2005). Red colours indicate interglacial and interstadial warm climate conditions

grew under favourable conditions during interglacial or interstadial periods (Table 2, Fig. 10), the linearly interpolated growth rates are then between 1.6 and 8.6 cm/ka for the stalagmites in the Steffisgang (cave level I) and about 3.4 cm/ka in the Labyrinth (cave level II). This falls within the range of most stalagmite growth rates measured in caves all over Europe (Geyh and Franke 1970; Hill and Forti 1997; Palmer 2007; Spötl and Boch 2019). The largest value given in Geyh and Franke (1970) is 50 cm/ka. However, under very rare conditions stalagmite growth rates may even reach a centimetre per year (Palmer 2007).

Using the highest growth rate determined for a stalagmite in the Erdmannshöhle under favourable interglacial/interstadial conditions (8.6 cm/ka), the growth of the largest stalagmite in cave level IIIa, the 4.5 m tall “Der Einsame”, would take about 52 ka, and with the largest growth rate taken from Geyh and Franke (1970), it would still take about 9 ka. For the largest stalactite in cave level III, i.e. the 3 m long “Der Grosse”, more than 10 ka seems to be a realistic estimate for its growth period.

6 Conceptual model for the Erdmannshöhle

Key-parameters for an evolution concept for the Erdmannshöhle are (1) the time span needed for the formation of cave passages after the breakthrough, which should be in the range of 20–30 ka, (2) the growth period needed for large speleothems such as “Der Einsame” and “Der Grosse”, which is more than 10 ka and up to more than 50 ka for the largest growth rates in the Erdmannshöhle, and (3) the results of U/Th dating, which give ages for the speleothem formation and minimum ages for the deposition of allochthonous clastic sands and gravels.

The conceptual model for the development of the Erdmannshöhle will be discussed within the framework of the recently revised Middle and Late Pleistocene glaciation history for Northern Switzerland (Fig. 11). The period after the so-called “Middle Pleistocene Reorganisation” (Preusser et al. 2011) comprises four or five glaciations which are referred to as Möhlin [MIS (Marine Isotope Stages) 10 \approx 337–374 ka or MIS 12 \approx 424–478 ka], Habsburg [MIS 8 \approx 240–300 ka or MIS 10 \approx 337–374 ka], Hagenholz [unsure] [MIS 8 \approx 240–300 ka], Beringen or Koblenz [MIS 6 \approx 130–190 ka] and Birrfeld [MIS 2–5d \approx 12–110 ka] (Martinson et al. 1987; Lisiecki and Raymo 2005; Graf 2009; Keller and Krays 2010; Preusser et al. 2011). The interglacials are Holstein

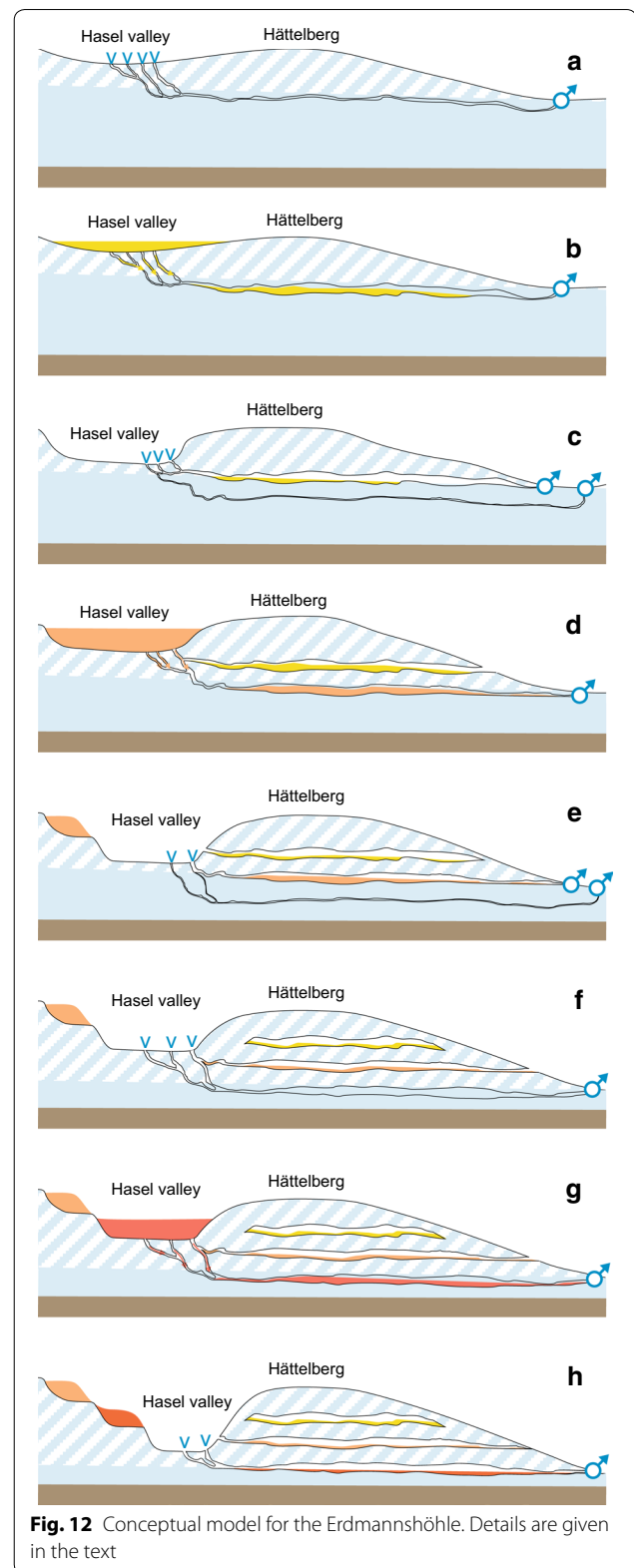


Fig. 12 Conceptual model for the Erdmannshöhle. Details are given in the text

[MIS 9 \approx 300–337 ka or MIS 11 \approx 374–424 ka], Meikirch [MIS 7 \approx 190–240 ka] and Eem [approx. MIS 5d \approx 110–130 ka] (Keller and Krayss 2010). A comparison with the Middle to Late Pleistocene stages for SW Germany after Ellwanger et al. (1999) and Habbe et al. (2007) is given in Table 1.

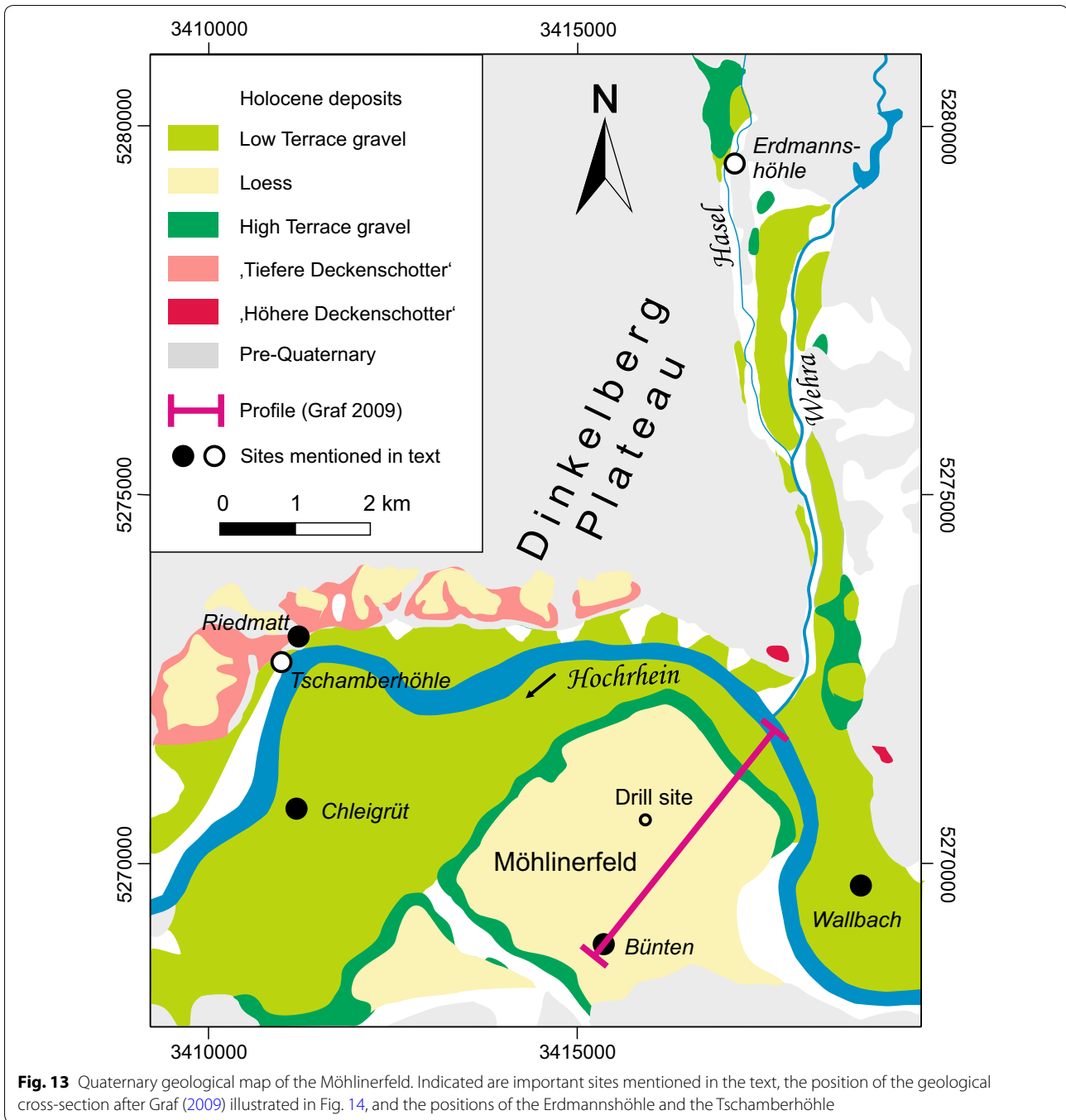
The early stages of the development of the Erdmannshöhle after the breakthrough may already have commenced during the Holstein Interglacial [MIS 9 or MIS 11], a warm period lasting 37 respectively 50 ka with very favourable conditions for karstification and speleogenesis (Fig. 12a). Partial filling of the cave level I with allochthonous gravels and sands probably occurred during a cold-to-warm transition, most likely at the end of the Habsburg (or questionable Hagenholz) Glacial and the beginning of the Meikirch Interglacial (Fig. 12b). The Meikirch Interglacial with temporary interstadial conditions (Keller and Krayss 2010) lasted over 50 ka and was a warmer period long enough for the formation of cave level II, whereas cave level I gradually became inactive (Fig. 12c). The Beringen Glaciation [MIS 6] was the period of the farthest known advance of the Wehratal glacier reaching as far as the Hochrhein valley, which brought the Hasel area to the close vicinity of a glacier. Some speleothem growth in the Steffisgang (cave level I) may point to the fact that harsh periglacial conditions with permafrost only arose during comparatively short periods. However, massive gravel deposits were accumulated during the Beringen Glaciation in the ancient Hasel valley and are now seen in the High Terrace (Figs. 1, 2). This event may also be responsible for the massive fill of cave level II with allochthonous, partly coarse-grained sands and gravels which is believed to have happened close to the end of the Beringen Glaciation and the early Eem Interglacial (Fig. 12d). The fill in many parts of the cave level II up to the ceiling persisted till the early stages of the Birrfeld Glacial [MIS 5c, d] as indicated by the U/Th dating in the Labyrinth. The gravel and sand fill were partly removed thereafter, probably with the onset of the formation of cave level IIIa (Troja, Verbindungsgang, Lehmhöhle) (Fig. 12e) and later on with cave level III (Fig. 12f). The formation of the cave levels IIIa and III presumably took place during the early Birrfeld warmer periods MIS 5c and MIS 5a and particularly during the Gossau Interstadial [MIS 3] (Fig. 11). During the main advance of the Birrfeld glaciers at MIS 2 karstification and speleogenesis ceased or slowed down during short periods of harsh periglacial conditions with permafrost. Gravel deposits were accumulated in the ancient Hasel valley and are now exposed as Lower Terrace gravels along the eastern flank and the southern tip of the Kaumberg (Figs. 1, 2). The age of these gravels near Hasel is unknown, however for the Hochrhein valley OSL dating

gives ages between 30 and 11 ka for the Lower Terrace gravels and sands (Kock et al. 2009). The mobilisation of large quantities of clastic sediments during the Birrfeld Glaciation [MIS 2] is most likely the source for the gravel deposits in the active Bachgang (cave level III) with a proven thickness of still >3 m (Piepjohn et al. 2005) (Fig. 12g). During the Holocene (MIS 1), the erosion of the late Birrfeld gravel deposits in the active Bachgang commenced (Fig. 12h), and perhaps a new cave level IV may have started to develop (Piepjohn 1987), although this has not yet been proven (Piepjohn et al. 2005).

7 Late pleistocene “cave level stratigraphy”—an attempt

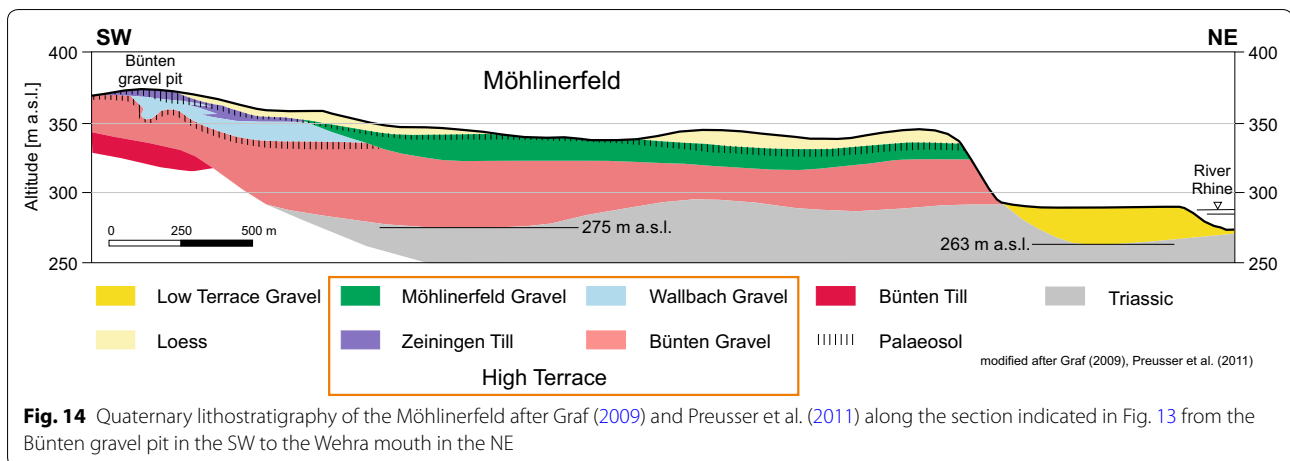
The Möhlinerfeld just 9 km to the south of the Erdmannshöhle (Fig. 13) is a key region for attempting to correlate cave levels with the sequence of Middle and Late Pleistocene deposits in the Hochrhein valley (Tschudi 1904; Dick et al. 1996; Müller-Dick 2000; Graf 2009; Keller and Krayss 2010; Preusser et al. 2011; Heuberger et al. 2014). The base of the Pleistocene deposits in the Möhlinerfeld, summarised as High Terrace, shows channel-like structures carved into Triassic bedrocks (Fig. 14). The oldest Pleistocene deposit is the Bünthen Till, a lodgement till with alpine material exposed in the south of the Möhlinerfeld. A palaeosol is not developed at the top of the Bünthen Till. The till is covered by the glaciofluvial Bünthen Gravel, which is predominantly built up of alpine components but showing pebbles and boulders originating from the Black Forest at the base. The top of the Bünthen Gravel is intensively weathered. The gravel components of the Wallbach Gravel on top of the Bünthen Gravel again show an alpine provenance. The Wallbach Gravel and the deeper units are intensively deformed by ice push. The Zeiningen Till at the top contains exclusively components from the Black Forest, indicating an advance of the Wehratal Glacier as far south as the Bünthen gravel pit where the extensively weathered till is exposed (Figs. 13, 14). To the N, the Zeiningen Till passes over into the Möhlinerfeld Gravel, which is dominated by alpine components but shows boulders and pebbles of Black Forest origin at the base. The top of the Möhlinerfeld Gravel is intensively weathered. The youngest deposits consist of loess on top of the High Terrace complex, reaching thicknesses up to 10 m, and Low Terrace gravels in the deeply incised Hochrhein valley (Figs. 13, 14).

There is general agreement that the Bünthen Till represents the furthest extent of alpine glaciers during the Middle Pleistocene, reaching the Möhlinerfeld during the Möhlin Glaciation (Graf 2009; Keller and Krayss 2010; Preusser et al. 2011). For Keller and Krayss (2010), the Bünthen Gravel is a remnant of the Habsburg Glaciation, whereas Graf (2009) points to the fact that



the lack of a palaeosol at the top of the Bünten Till excludes deposition during an independent glaciation. Thus, Graf (2009) assumes that the Bünten Till and Bünten Gravel must both have been deposited during the Möhlin Glaciation. Following Preusser et al. (2011), the intense weathering and palaeosol formation at the top of the Bünten Gravel indicates interglacial conditions, which Keller and Krayss (2010) correlate with the palynostratigraphic profile at Riedmatt (Fig. 13)

(Bludau et al. 1994). However, the pollen spectrum at Riedmatt does not support true interglacial conditions because of the dominance of boreal forest vegetation with *Picea*, *Pinus* and *Betula* alternating with steppe vegetation. Because the sample site at Riedmatt is covered by High Terrace gravels, and interglacial conditions are not seen in the pollen spectrum, the profile reflects interstadial conditions within the Riss Glaciation (cf. Table 1) (Bludau et al. 1994), i.e. between the



Habsburg and the Beringen/Koblenz Glaciations. Some weathering at the top section of the Wallbach Gravel may point to another warmer period between the Habsburg and Beringen/Koblenz Glaciations (Graf 2009). General agreement exists with regard to the Zeiningen Till and the Möhlinerfeld Gravel, which are both remnants of the Beringen/Koblenz Glaciation with a 2 to 3 m, deeply weathered palaeosol on top reflecting interglacial conditions of the Eem Interglacial (Keller and Krayss 2010). At the top of the High Terrace complex, loess was deposited during the Birrfeld Glaciation. Based on OSL and IRSL (infrared stimulated luminescence) dating, loess samples taken from a drill site just at the centre of the Möhlinerfeld (Fig. 13) give ages between 19.5 and 68.1 ka, with a main loess accumulation period between 30 and 35 ka (Gaar and Preusser 2017). The oldest loess date refers to an early advance (Untersee Stadial after Keller and Krayss 2010) at MIS 4, separated from the period of main loess accumulation by decalcified loess (Gaar and Preusser 2017), which points to warmer, interstadial conditions (Gosau Interstadial after Preusser et al. 2011). The Low Terrace gravels which are dated using OSL at the Chleigrüt gravel pit (Fig. 13) with 26.7 to 18.3 ka and at Wallbach with 27.5 ± 1.7 ka (Kock 2008, Kock et al. 2009) are exclusively aged as Late Pleistocene in the western Hochrhein valley.

With respect to the evolution of the Erdmannshöhle (cf. Chapter 6), we would suggest the following correlation with the Möhlinerfeld evidence (Fig. 15):

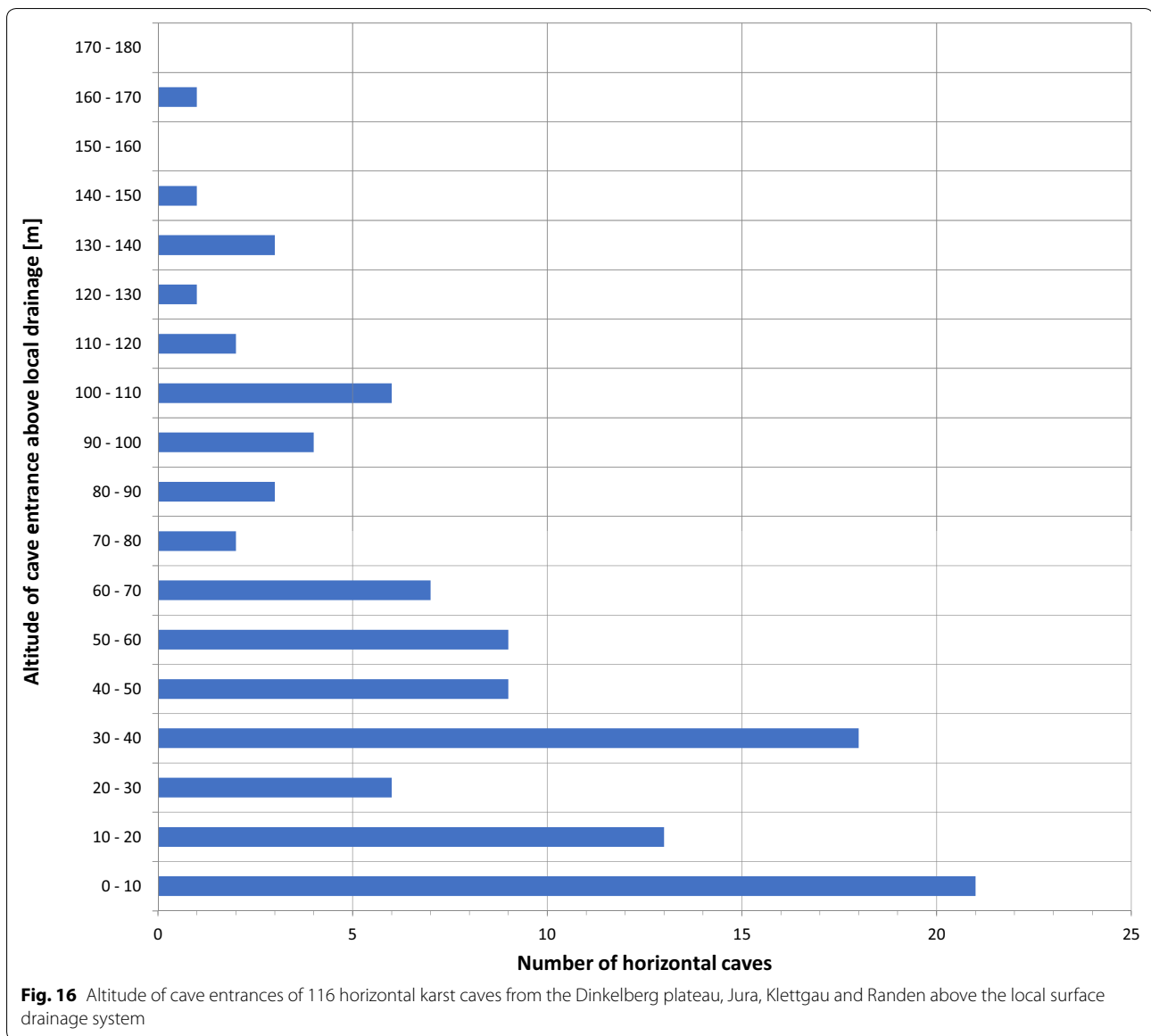
1. Development of cave level I during the period of strong weathering at the top of the Bünten Gravel, most likely the Holstein Interglacial.
2. Partial fill of cave level I with allochthonous sediments during a cold-to-warm transition, which could

be correlated with the Wallbach Gravel of possible Habsburg age.

3. The weakly weathered surface of the Wallbach Gravel can be correlated with an interstadial such as seen in Riedmatt (Bludau et al. 1994) or an interglacial (Meikirch), which we would correlate with the onset of the development of cave level II and the termination of the active stage of cave level I with sediment erosion at the phreatic-vadose transition.
4. The fill of cave level II with allochthonous sediments mainly at the end of the Beringen Glaciation, which can be correlated with the Möhlinerfeld Gravel.
5. The erosion of sediments in cave level II commenced in the Eem Interglacial and lasted up to the early Birrfeld Glaciation, which can be correlated approximately with the palaeosol of the Eem Interglacial (and early Birrfeld Glaciation?) at the top of the Möhlinerfeld Gravel. The early stages of the development of cave level IIIa/III fell approximately in the early Birrfeld Glaciation.
6. The main development of cave level IIIa/III was during the early and middle Birrfeld Glaciation, and sediment fill mainly occurred close to the end of the Birrfeld Glaciation. This correlates with the loess and Low Terrace gravels in the Möhlinerfeld.
7. Finally, erosion of the allochthonous sediments in cave level III started in the Holocene, which correlates with the onset of cave evolution in the Tschamberhöhle (Kock et al. 2009) just NW of the Möhlinerfeld (Fig. 13).

8 Caves as an archive for quaternary research

Age dating with the U/Th method combined with stable isotope investigations on speleothems provide an insight into the palaeo-climate of the interglacials such as the

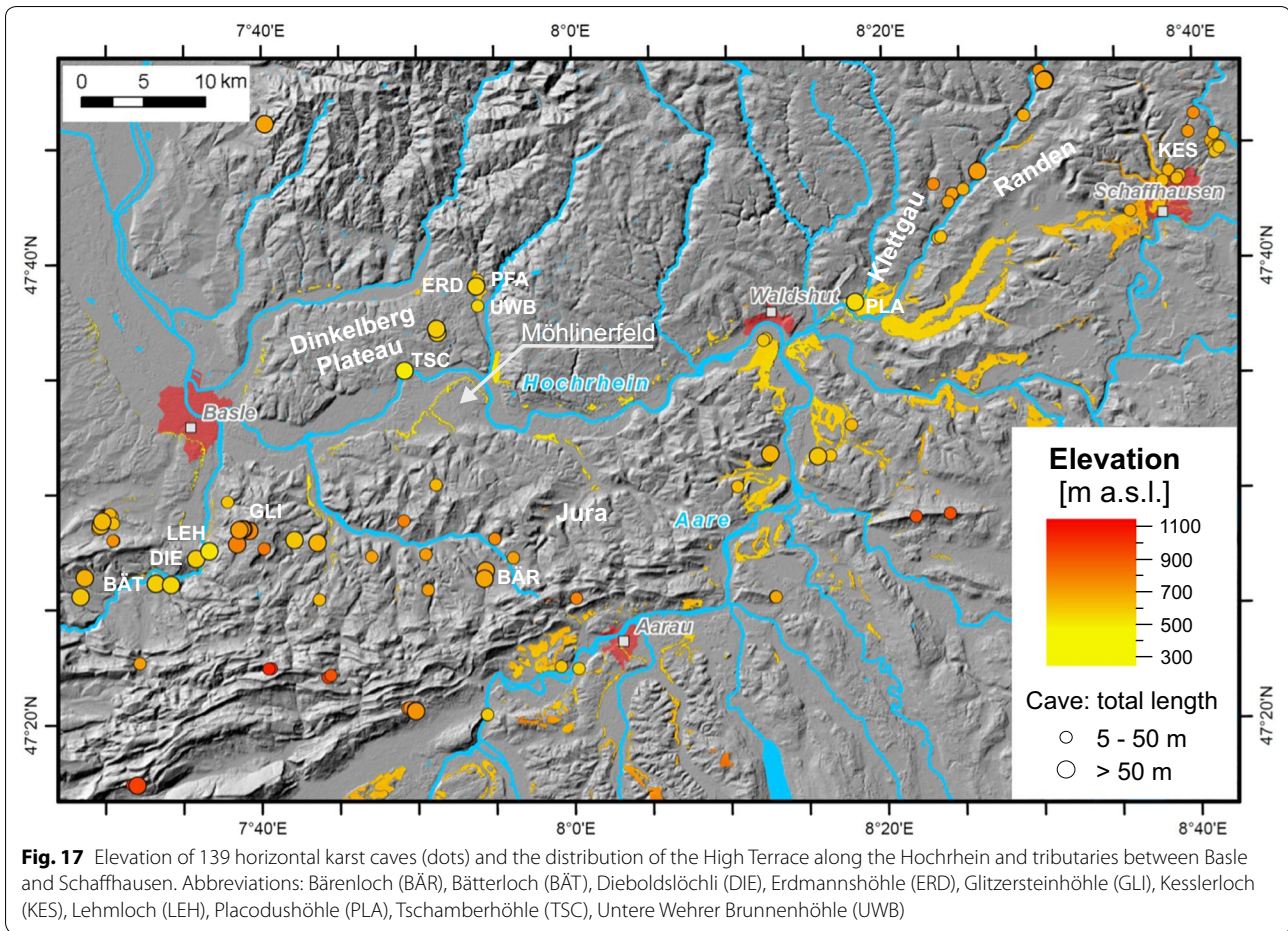


a comparatively short period. Thus, speleothems are a powerful archive for the reconstruction of the Pleistocene climate history.

Furthermore, allochthonous clastic cave deposits can be dated either by the organic content in Late Pleistocene and Holocene deposits with the radiocarbon method or directly with the OSL/IRSL methods and cosmogenic isotopes (Zhang et al. 2010; Granger and Fabel 2019). By combining these methods, it is possible to date various types of sediments covering the entire Quaternary. Coarse-grained sand and gravel deposits are of particular interest because they are deposited by a cave stream. In the case of a water-table cave like the Erdmannshöhle, this is near the phreatic surface. By dating such cave

deposits at different cave altitudes or in a single cave at different levels, the lowering of the phreatic surface due to the incision of the local surface drainage systems as a consequence of land uplift and fluvial erosion can be reconstructed (Häuselmann et al. 2007).

Due to lack of absolute age dates, it is only possible for the region on both sides of the Hochrhein, i.e. the Dinkelberg plateau, Jura, Klettgau and Randen, to estimate the relative ages of caves based on their relative height above the recent surface drainage (Fig. 16), assuming that these caves originally developed at the phreatic surface. Three clear peaks in the histogram (Fig. 16) are visible summarising 106 elevations of the entrances of horizontal caves with lengths between 5 and 2300 m: a first one slightly



above the recent surface drainage system at around 5 m, a second one at around 35 m and finally a third weak peak at around 105 m. The caves just above the recent surface drainage system are probably the youngest caves developed during the Middle and Late Pleistocene. The caves above are likely to be older, maybe early Pleistocene. There are even caves, probably the oldest ones, that cannot be related to a recent surface drainage system (and are thus not included in Fig. 16), because they are situated in high ground in the Jura Mountains on isolated plateaus. However, the interpretation of Fig. 16 is based purely on a statistical approach, which for instance does not exclude caves in a perched karst that are located clearly above the recent surface drainage system but are young as well.

Figure 17 shows the location of 139 horizontal karst caves in the region together with the elevation of the top of the High Terrace in Northern Switzerland and SW Germany. Most of them are small caves with a maximum length up to 50 m. However, 18 caves have a length between 50 and 100 m and 14 more than 100 m and up to 2300 m. Some of them are rich in sinter formations and

clastic sediments. Horizontal karst caves with an elevation below the top of the High Terrace are assumed to be young, i.e. Middle Pleistocene and younger. This has been proven for the Erdmannshöhle, the Tschamberhöhle (cf. Figures 1, 4, 17) and the Placodushöhle, and it also seems to hold true for the Pfarrhaushöhle, the Untere Wehrer Brunnenhöhle and the Lehmloch (Figs. 1, 17). However, most caves are located well above the High Terrace, which might point to high ages beyond the Middle Pleistocene.

Exploring the cave archive as part of Quaternary research has not really started yet. Currently, age dating using radiocarbon or the U/Th method are published only for seven of more than 250 known caves in the region. Aside from the Erdmannshöhle, these are the Bättlerloch, Dieboldslöchli, Glitzersteinhöhle, Bärenloch, Tschamberhöhle and Kesslerloch (Ammann et al. 1988; Lemeille et al. 1999; Schmidt et al. 2001; Becker 2005; Kock 2008; Kock et al. 2009; Becker et al. 2012) (Fig. 17). Sedimentologists have carried out barely any investigations of allochthonous cave deposits, and only

archaeologists pushed for palynostratigraphy. Surely, the cave archive deserves more attention in Quaternary research.

9 Summary

For the first time, U/Th dating on speleothems was carried out in the Erdmannshöhle, providing information that can be used to pinpoint the chronology of the speleogenetic and depositional processes of the cave within the framework of modern Middle to Late Pleistocene stratigraphy. It seems possible to directly correlate the evolution of the cave based on the formation of cave levels and the timing of the deposition of allochthonous clastic sediments with the High and Low Terrace stratigraphy in the Hochrhein valley. There are many more caves in Northern Switzerland and SW Germany that deserve more detailed studies with respect to modern sedimentology, stable isotope analyses and dating using different methods. Caves may launch a new field of activity for Quaternary research, because the cave archive is well protected against surface processes such as erosion, weathering and alteration, and most caves are young, i.e. Late Miocene to Holocene.

Acknowledgements

We gratefully acknowledge the community of Hasel, particularly mayor Helmut Kima, for facilitating the investigations in the Erdmannshöhle. We thank Hubert Saaler, Kurt Zimmermann and Thomas Singeisen for their guidance and active support in the cave during sampling. Hennes Obermeyer gave valuable information concerning the cave and supplied a first flowstone sample for U/Th dating. Th/U dating was performed at the Institute of Environmental Physics with the help of René Eichstädter and through support of Norbert Frank. Florian Kober and Marco Filipponi helped to significantly improve the manuscript and Andreas Ludwig prepared Fig. 17. Finally, we wish to thank Philipp Häuselmann (SISKA) for the critical review of the first draft of our manuscript and Angela Paulsen and Linda McKinley for improvements in native speaking English.

Authors' contributions

AB was responsible for the organisation of the sampling campaign in the cave. ASR carried out the U/Th dating at Universität Heidelberg. KP supplied the cave map, the geological map of the Hasel area and basic data concerning the geology of the karst environment. AB wrote the manuscript aside from Chapter 4.2, which was written by ASR. All illustrations were prepared for publication by AB, Table 1 by KP and Table 2 by ASR. All authors read and approved the final manuscript.

Funding

We wish to thank Nagra for the financial support of the project. The primary target was to correlate the cave levels with the Late Pleistocene terraces in the Hochrhein valley to quantify rates of lowering of the receiving stream level.

Availability of data and materials

The results of U/Th dating are stored at Universität Heidelberg, Institut für Umweltphysik, under the laboratory code and sample numbers given in Table 2. All U/Th dating from the Erdmannshöhle are included in Table 2. Further sources of information concerning the interpretation of data are published data included in the reference list.

Competing interests

The authors declare that they have no competing interests.

Author details

¹ Max-Planck-Str. 6, 76351 Linkenheim-Hochstetten, Germany. ² Bundesanstalt für Geowissenschaften und Rohstoffe, Stilleweg 2, 30655 Hannover, Germany. ³ Institut für Umweltphysik, Universität Heidelberg, Im Neuenheimer Feld 229, 69120 Heidelberg, Germany.

Received: 1 October 2019 Accepted: 23 May 2020

Published online: 26 June 2020

References

- Abel, T. (2003). Untersuchungen zur Genese des Malmkarsts der Mittleren Schwäbischen Alb im Quartär und jüngeren Tertiär. *Tübinger Geowissenschaftliche Arbeiten*, C 67, p.187.
- Abel, T., Hinderer, M., & Sauter, M. (2002). Karst genesis of the Swabian Alb, south Germany, since the Pliocene. *Acta Geologica Polonica*, 52(1), 43–54.
- Ammann, B., Bandi, H.-G., Buser, M., Chaix, L., Joos, M., Mäglin, T., et al. (1988). Neue Untersuchungen am Kesslerloch bei Thayngen. *Antiqua*, 17, pp. 128.
- Arps, J. (2017). *Towards ε-precision of U-series age determinations of secondary carbonates*. PhD Thesis, University Heidelberg. <https://doi.org/10.11588/heidok.00023313>.
- Audra, P., & Palmer, A. N. (2011). The pattern of caves: controls of epigenic speleogenesis. *Géomorphologie Relief Processus Environment*, 17(4), 359–378.
- Becker, A. (2005). Radiokohlenstoff-Altersdatierungen an Sedimenten der Glitzersteinhöhle. *d'Höhlenperle*, 2005, pp. 28–33.
- Becker, A., Häuselmann, P., Eikenberg, J., & Gilli, E. (2012). Active tectonics and earthquake destructions in caves of northern and central Switzerland. *International Journal of Speleology*, 41(1), 35–49.
- Bludau, W., Groschopf, R., & Schreiner, A. (1994). Ein Riß-Interstadial bei Riedmatt am Hochrhein. *Jahresberichte und Mitteilungen des oberrheinischen geologischen Vereins*, N.F. 76, pp. 295–323.
- Böcker, T. (1969). Karstic water research in Hungary. *Bulletin of the International Association of Scientific Hydrology*, XIV(4-12), pp. 7–20.
- Bridgland, D. R., & Westaway, R. (2007). Climatically controlled river terrace staircases: a worldwide Quaternary phenomenon. *Geomorphology*, 98(3-4), 285–315.
- Cheng, H., Edwards, R. L., Hoff, J., Gallup, C. D., Richards, D. A., & Asmerom, Y. (2000). The half-lives of uranium-234 and thorium-230. *Chemical Geology*, 169, 17–33.
- Cheng, H., Fleitmann, D., Edwards, R. L., Wang, X., Cruz, F. W., Auler, A. S., et al. (2009). Timing and structure of the 8.2 kyr B.P. event inferred from $\delta^{18}\text{O}$ records of stalagmites from China, Oman, and Brazil. *Geology*, 37, 1007–1010.
- Claude, A., Akçar, N., Ivy-Ochs, S., Schlunegger, F., Kubik, W. P., Dehnert, A., et al. (2017). Timing of early Quaternary gravel accumulation in the Swiss Alpine foreland. *Geomorphology*, 276, 71–85.
- Delisle, G., Caspers, G., & Freund, H. (2003). Permafrost in north-central Europe during the Weichselian: how deep? In M. Phillips, S. M. Springman & L. U. Aronson (Eds.), *Permafrost* (pp. 187–191). 8th Int. Conf. on Permafrost, Zurich, July 2003.
- Dick, K. A., Graf, H. R., Müller, B. U., Hartmann, P., & Schlüchter, C. (1996). Das nordalpine Wasserschloss und seine eiszeitgeologische Umgebung. *Eclogae Geologicae Helveticae*, 89(1), 635–645.
- Douville, E., Sallé, E., Frank, N., Eisele, M., Pons-Branchu, E., & Ayrault, S. (2010). Rapid and accurate U-Th dating of ancient carbonates using inductively coupled plasma-quadrupole mass spectrometry. *Chemical Geology*, 272, 1–11.
- Dreybrodt, W. (1988). *Processes in karst systems—physics, chemistry, and geology*. Berlin: Springer.
- Dreybrodt, W., & Gabrovšek, F. (2000). Dynamics of the evolution of single karst conduits. In A. B. Klimchouk, D. C. Ford, A. N. Palmer, & W. Dreybrodt (Eds.), *Speleogenesis—evolution of karst aquifers* (pp. 184–193). Huntsville: National Speleological Society.
- Ellwanger, D., Fiebig, M., & Heinz, J. (1999). Quartärgeologie des mittleren Rheingletschergebietes. *Jahresberichte und Mitteilungen des oberrheinischen geologischen Vereins*, N.F. 81, pp. 217–230.
- Fairchild, I. J., & Baker, A. (2012). *Speleothem science—from process to past environments*. Chichester: Wiley.

- Faulkner, T. (2006). Limestone dissolution in phreatic conditions at maximum rates and in pure, cold water. *Cave and Karst Science*, 33(1), 11–20.
- Filipponi, M. (2003). Bruchmechanismen der Inkasion. *AGS. Info*, 2(03), 42–49.
- Fleitmann, D., & Matter, A. (2009). The speleothem record of climate variability in Southern Arabia. *Geoscience*. <https://doi.org/10.1016/j.crte.2009.01.006>.
- Ford, D. C., & Ewers, R. O. (1978). The development of limestone cave systems in the dimensions of length and depth. *Canadian Journal of Earth Sciences*, 15, 1783–1798.
- Gaar, D., & Preusser, F. (2017). Age of the most extensive glaciation of northern Switzerland: evidence from the scientific drilling at Möhliner Feld. *E & G Quaternary Science Journal*, 61(1), 1–5.
- Geyh, M. A., & Franke, H. W. (1970). Zur Wachstumsgeschwindigkeit von Stalagmiten. *Atompaxis*, 16(1), 1–3.
- Govaerts, J., Beerten, K., & ten Veen, J. (2016). Weichselian permafrost depth in the Netherlands: a comprehensive uncertainty and sensitivity analysis. *The Cryosphere*, 10, 2907–2922.
- Graf, H. R. (2009). Stratigraphie von Mittel- und Spätpleistozän in der Nordschweiz. *Beiträge zur geologischen Karte der Schweiz* (N.F.), 168, pp. 198.
- Granger, D. E., & Fabel, D. (2019). Cosmogenic isotope dating. In W. White, D. Culver, & T. Pipan (Eds.), *Encyclopedia of caves* (3rd ed., pp. 348–352). Amsterdam: Academic Press.
- Griffiths, M. L., Drysdale, R. N., Gagan, M. K., Frisia, S., Zhao, J.-X., Ayliffe, L. K., et al. (2010). Evidence for Holocene changes in Australian-Indonesian monsoon rainfall from stalagmite trace element and stable isotope ratios. *Earth and Planetary Science Letters*, 292(1–2), 27–38.
- Habbe, K. A., Ellwanger, D., & Becker-Haumann, R. (2007). Stratigraphische Begriffe für das Quartär des süddeutschen Alpenvorlandes. *Eiszeitalter und Gegenwart*, 56(1–2), 66–83.
- Häberli, W. (2010). Glaciological conditions in northern Switzerland during recent Ice Ages. *Nagra Arbeitsbericht*, NAB 10–18, pp. 28.
- Häuselmann, P., Granger, D. E., Jeannin, P.-Y., & Lauritzen, S.-E. (2007). Abrupt glacial valley incision at 0.8 Ma dated from cave deposits in Switzerland. *GSA*, 35(2), 143–146.
- Hantke, R. (1978–83). *Eiszeitalter—Die jüngste Erdgeschichte der Alpen und ihrer Nachbargebiete*. 3 vol, Thun: Ott.
- Harmand, D., Adamson, K., Rixhon, G., Jaillet, S., Loson, B., Devos, A., et al. (2017). Relationships between fluvial evolution and karstification related to climatic, tectonic and eustatic forcing in temperate regions. *Quaternary Science Reviews*, 166, 38–56.
- Häuselmann, P. (2002). Cave genesis and its relationship to surface processes: Investigations in the Siebenhengste region (BE, Switzerland). *Höhlenforschung im Gebiet Siebenhengste*, 6, pp. 168.
- Heuberger, S., Büchi, M., & Naef, H. (2014). Drainage system and landscape evolution of northern Switzerland since the late Miocene. *Nagra Arbeitsbericht*, NAB 12–20, pp. 102.
- Hill, C., & Forti, P. (1997). *Cave minerals of the world* (2nd ed.). Huntsville: National Speleological Society.
- Hoffmann, D. L., Prytulak, J., Richards, D. A., Elliott, T., Coath, C. D., Smart, P. L., et al. (2007). Procedures for accurate U and Th isotope measurements by high precision MC-ICPMS. *International Journal of Mass Spectrometry and Ion Physics*, 264(2–3), 97–109.
- Hoffmann, D. L., Standish, C. D., Garcia-Diez, M., Pettitt, P. B., Milton, J. A., Zilhao, J., et al. (2018). U-Th dating of carbonate crusts reveals Neandertal origin of Iberian cave art. *Science*, 359(6378), 912–915.
- Keller, O., & Krayss, E. (2010). Mittel- und spätpleistozäne Stratigraphie und Morphogenese in Schlüsselregionen der Nordschweiz. *E & G Quaternary Science Journal*, 59(1–2), 88–119.
- Kempe, S., Rosendahl, W., Wiegand, B., & Eisenhauer, A. (2002). New speleothem dates from caves in Germany and their importance for the Middle and Upper Pleistocene climate reconstruction. *Acta Geologica Polonica*, 52(1), 55–61.
- Kock, S. (2008). *Pleistocene terraces in the Hochrhein area—formation, age constraints and neotectonic implications* (p. 99). Basel: Diss. Univ.
- Kock, S., Huggenberger, P., Preusser, F., Rentzel, P., & Wetzel, A. (2009). Formation and evolution of the Lower Terrace of the Rhine river in the area of Basel. *Swiss Journal of Geosciences*, 102, 307–321.
- Lemeille, F., Cushing, M., Carbon, D., Grellet, B., Bitterli, T., Flehoc, C., et al. (1999). Co-seismic ruptures and deformations recorded by speleothems in the epicentral zone of the Basel earthquake. *Geodinamica Acta*, 12(3–4), 179–191.
- Lignier, V., & Desmet, M. (2002). Les archives sédimentaires quaternaires de la grotte sous les Sangles (Bas-Gugey, Jura méridional, France) – Indices paléo-climatiques et sismo-tectoniques. *Karstologia*, 39(1), 27–46.
- Lisiecki, L. E., & Raymo, M. E. (2005). A Pliocene-Pleistocene stack of 57 globally distributed benthic $\delta^{18}\text{O}$ records. *Paleoceanography*. <https://doi.org/10.1029/2004PA001071>.
- Lutz, M. (1964). Stratigraphische und tektonische Untersuchungen am südwestlichen Schwarzwaldrand zwischen Wiesental und Hochrhein. *Oberrheinische geologische Abhandlungen*, 13, 75–122.
- Martinson, D. G., Pisias, N. G., Hays, J. D., Imbrie, J., Moore, T. C., & Shackleton, N. J. (1987). Age dating and the orbital theory of the Ice Ages: development of a high-resolution 0 to 300,000-year chronostratigraphy. *Quaternary Research*, 27, 1–29.
- Matos, L., Mienis, F., Wienberg, C., Frank, N., Kwiatkowski, C., Groeneveld, J., et al. (2015). Interglacial occurrence of cold-water corals off Cape Lookout (NW Atlantic): first evidence of the Gulf Stream influence. *Deep Sea Research Part I: Oceanographic Research Papers*, 105, 158–170.
- Müller-Dick, K. A. (2000). Möhliner Feld im Hochrheintal. In M. Kelly, U. Linden & C. Schlüchter (Eds.), *Exkursionsführer, Exkursion A1, DEUQUA*. 6.-8.9.2000, Bern, pp. 10–13.
- Palmer, A. N. (1991). Origin and morphology of limestone caves. *Bulletin of the Geological Society of America*, 103, 1–21.
- Palmer, A. N. (2000). Digital modeling of individual solution conduits. In A. B. Klimchouk, D. C. Ford, A. N. Palmer, & W. Dreybrodt (Eds.), *Speleogenesis—evolution of karst aquifers* (pp. 194–200). Huntsville: National Speleological Society.
- Palmer, A. N. (2007). *Cave geology*. Lawrence, Kansas: Allen Press.
- Penck, A. & Brückner, E. (1901–09). *Die Alpen im Eiszeitalter*. 3 vol, Leipzig: Tauchnitz.
- Piepjoh, K. (1987). *Geologische Neukartierung im südwestlichen Schwarzwald nördlich von Wehr (Dinkelberg/Hotzenwald* (p. 121). Baden-Württemberg): Diplom-Arbeit Universität Hamburg.
- Piepjoh, K. (1995a). Die Erdmannshöhle bei Hasel (Südbaden) und die Abhängigkeit ihrer Entwicklung von den quartären Klima-Ereignissen. *Münstersche Forschung zur Geologie und Paläontologie*, 77, 155–171.
- Piepjoh, K. (1995b). Karsthydrographie im Bereich der Ortschaft Hasel nördlich von Wehr (Südbaden). *Münstersche Forschung zur Geologie und Paläontologie*, 77, 173–184.
- Piepjoh, K., Lacher, F., Hermann, R., Siegener, U., & Zimmermann, K. (2005). Die Erdmannshöhle bei Hasel, Südbaden. *Mitteilungen des Verbandes deutscher Höhlen- und Karstforscher*, 51(3), 84–92.
- Preusser, F., Graf, H. R., Keller, O., Krayss, E., & Schlüchter, C. (2011). Quaternary glaciation history of northern Switzerland. *E & G Quaternary Science Journal*, 60(2–3), 282–305.
- Quinif, Y. (2006). Complex stratigraphic sequences in Belgian caves—correlation with climatic changes during the Middle, the Upper Pleistocene and the Holocene. *Geologica Belgica*, 9(3–4), 231–244.
- Sauvet, G., Bourrillon, R., Conkey, M., Fritz, C., Gárate-Maidagan, D., Rivero Vilá, O., et al. (2017). Uranium/thorium dating method and Palaeolithic rock art. *Quaternary International*, 432, 86–92.
- Schmidt, E., Mohler, W. A. & Sedlmeier, J. (2001). Die Höhle Bärenloch bei Tecknau/Wenslingen—Die Grabungen 1962–1968. *Archäologie und Museum*, 42, p. 43.
- Siegener, U. (1994). Die Erdmanns Höhle bei Hasel—Ein Beitrag zur Speläologie (Höhlenkunde) des Haseler Karstes. *Das Markgräflerland*, 2(94), 345–367.
- Spötl, C., & Boch, R. (2019). Uranium series dating of speleothems. In W. White, D. Culver, & T. Pipan (Eds.), *Encyclopedia of caves* (3rd ed., pp. 1096–1102). Amsterdam: Academic Press.
- Spötl, C., & Cheng, H. (2014). Holocene climate change, permafrost and cryogenic carbonate formation: insights from a recently deglaciated, high-elevation cave in the Austrian Alps. *Climate of the Past*, 10(4), 1349–1362.
- Tschudi, R. (1904). *Zur Altersbestimmung der Moränen im untern Wehrtaale* (p. 29). Basel: Diss. Univ.
- Wefing, A.-M., Arps, J., Blaser, P., Wienberg, C., Hebbeln, D., & Frank, N. (2017). High precision U-series dating of scleractinian cold-water corals using an automated chromatographic U and Th extraction. *Chemical Geology*, 475, 140–148.
- Wenz, S., Scholz, D., Sürmelihindi, G., Passchier, C. W., Jochum, K. P., & Andreae, M. O. (2016). $^{230}\text{Th}/\text{U}$ -dating of carbonate deposits from ancient aqueducts. *Quaternary Geochronology*, 32, 40–52.

- White, W. B. (1988). *Geomorphology and hydrology of karst terrains*. New York: Oxford University Press.
- White, E. L. (2005). Breakdown.- In D. C. Culver & W. B. White (Ed.), *Encyclopedia of caves (2nd edition)* (pp. 56-60), Amsterdam: Elsevier.
- Zhang, J.-F., Huang, W.-W., Yuan, B.-Y., Fu, R.-Y., & Zhou, L.-P. (2010). Optically stimulated luminescence dating of cave deposits at the Xiaogushan pre-historic site, northeastern China. *Journal of Human Evolution*, 59, 514–524.
- Zhao, K., Wang, Y., Edwards, R. L., Cheng, H., & Liu, D. (2010). High-resolution stalagmite $\delta^{18}\text{O}$ records of Asian monsoon changes in central and southern

China spanning the MIS 3/2 transition. *Earth and Planetary Science Letters*, 298(1–2), 191–198.

Publisher's Note

Springer Nature remains neutral with regard to jurisdictional claims in published maps and institutional affiliations.

Submit your manuscript to a SpringerOpen[®] journal and benefit from:

- ▶ Convenient online submission
- ▶ Rigorous peer review
- ▶ Open access: articles freely available online
- ▶ High visibility within the field
- ▶ Retaining the copyright to your article

Submit your next manuscript at ▶ [springeropen.com](https://www.springeropen.com)
